JGR Atmospheres

RESEARCH ARTICLE
10.1029/2024JD041072

Relating Dimethyl Sulphide and Methanethiol Fluxes to Surface Biota in the South-West Pacific Using Shipboard Air-Sea Interface Tanks

M. Rocco[1,2,3], E. Dunne[4], R. Salignat[1], A. Saint-Macary[5,6], M. Peltola[1,7], T. Barthelmeß[8], G. Chamba[1], N. Barr[5], K. Safi[9], A. Marriner[5], S. Deppeler[5], C. Rose[1], J. Uitz[10], J. Harnwell[4], A. Engel[8], A. Colomb[1], A. Saiz-Lopez[11], M. J. Harvey[5†], C. S. Law[5,6], and K. Sellegri[1]

[1]Université Clermont Auvergne, CNRS, Laboratoire de Météorologie Physique (LaMP), Aubière, France, [2]Now at Aix Marseille University, CNRS, LCE, Marseille, France, [3]CNRS, Aix Marseille University, IRD, Avignon University, IMBE, Marseille, France, [4]CSIRO Environment, Aspendale, VIC, Australia, [5]National Institute of Water and Atmospheric Research, Wellington, New Zealand, [6]Department of Marine Science, University of Otago, Dunedin, New Zealand, [7]Now at INAR, University of Helsinki, Helsinki, Finland, [8]GEOMAR Helmholtz Centre for Ocean Research Kiel, Kiel, Germany, [9]National Institute of Water and Atmospheric Research, Hamilton, New Zealand, [10]Laboratoire d'Océanographie de Villefranche, Villefranche-sur-Mer, France, [11]Department of Atmospheric Chemistry and Climate, Institute of Physical Chemistry Blas Cabrera, CSIC, Madrid, Spain

†Deceased

Key Points:

- Ratio of methanethiol (MeSH) to dimethyl sulphide (DMS) fluxes of 11%–18% is consistent across different water types in Southern Ocean waters
- Significant correlations between DMS_w and $MeSH_w$ and nanophytoplankton were observed, enabling development of parameterizations for models

Supporting Information:

Supporting Information may be found in the online version of this article.

Correspondence to:

K. Sellegri and M. Rocco,
karine.sellegri@uca.fr;
rocco.manon@gmail.com

Citation:

Rocco, M., Dunne, E., Salignat, R., Saint-Macary, A., Peltola, M., Barthelmeß, T., et al. (2025). Relating dimethyl sulphide and methanethiol fluxes to surface biota in the south-west Pacific using shipboard air-sea interface tanks. *Journal of Geophysical Research: Atmospheres*, *130*, e2024JD041072. https://doi.org/10.1029/2024JD041072

Received 28 FEB 2024
Accepted 13 DEC 2024

Author Contributions:

Conceptualization: M. Rocco, E. Dunne, M. Peltola, A. Marriner, M. J. Harvey, C. S. Law, K. Sellegri
Data curation: M. Rocco, E. Dunne, A. Saint-Macary, T. Barthelmeß, G. Chamba, S. Deppeler, J. Uitz, J. Harnwell, A. Engel, A. Colomb, M. J. Harvey
Formal analysis: M. Rocco, E. Dunne, R. Salignat, A. Saint-Macary, M. Peltola, T. Barthelmeß, G. Chamba, N. Barr, M. J. Harvey, C. S. Law, K. Sellegri

Abstract Dimethyl sulphide (DMS) and methanethiol (MeSH) emissions from South Pacific surface seawater were determined in deck board Air-Sea Interface Tanks during the Sea2Cloud voyage in March 2020. The measured fluxes from water to headspace (F) varied with water mass type, with lowest fluxes observed with Subtropical and Subantarctic waters and highest fluxes from Frontal waters. Measured DMS fluxes were consistent with fluxes calculated using a two-layer model and seawater DMS concentrations. The MeSH:DMS flux ratio was 11%–18% across the three water mass types, confirming that MeSH may represent a significant unaccounted contribution to the atmospheric sulfur budget, with potentially important implications for marine aerosol formation and growth in models. Combining data from the ASITs and ambient surface seawater identified significant Spearman rank correlations for both dissolved DMS and MeSH with nanophytoplankton cell abundance ($p_{value} < 0.012$), suggesting an important role for this phytoplankton size class in determining regional DMS and MeSH emissions. Applying a nanophytoplankton-based parameterization to estimate DMS_w provided good agreement with a recent DMS climatology. Consequently, the observed relationship between DMS_w, $MeSH_w$ and nanophytoplankton cell abundances may be applicable for modeling atmospheric fluxes.

Plain Language Summary In March 2020, researchers conducted experiments during the Sea2Cloud voyage east of New Zealand in which they measured the emissions of the climate relevant gases dimethyl sulphide (DMS) and methanethiol (MeSH). These sulfur gases are produced by marine microorganisms and their emissions were measured in tanks containing different sea water types. Lowest emissions were observed in Subtropical and Subantarctic waters while the highest were in Frontal waters where Subantarctic and Subtropical seawaters meet and support large phytoplankton blooms. While DMS has been extensively studied, there are far fewer measurements of MeSH which this study confirmed be a significant, relatively constantly scaled to DMS and previously underestimated contributor to atmospheric sulfur levels with potential implications for climate. The study established significant correlations between DMS and MeSH fluxes and nanophytoplankton cell abundance, highlighting the importance of this phytoplankton size class in marine emissions to the atmosphere. The results presented here can help constrain emissions of these sulfur gases in climate models.

1. Introduction

Oceanic emission of dimethyl sulphide (DMS) is considered the largest natural source of atmospheric sulfur, with the global flux estimated at 23–35 Tg S yr^{-1} (Hulswar et al., 2022; Lana et al., 2011; Simó & Dachs, 2002). In the remote marine atmosphere, the oxidation of DMS leads to the formation of sulfuric acid, which is considered to be a key species for aerosol nucleation in other environments (Fung et al., 2022), and a major source of cloud condensation nuclei (CCN) in the remote marine atmosphere (Korhonen et al., 2008). The CLAW hypothesis (Charlson et al., 1987) proposed that enhanced DMS emissions would lead to higher numbers of CCN and so

Funding acquisition: C. S. Law, K. Sellegri
Investigation: M. Rocco, E. Dunne, R. Salignat, A. Saint-Macary, T. Barthelmeß, G. Chamba, N. Barr, K. Safi, J. Uitz, M. J. Harvey, C. S. Law, K. Sellegri
Methodology: M. Rocco, E. Dunne, M. Peltola, N. Barr, A. Marriner, S. Deppeler, C. Rose, M. J. Harvey, C. S. Law, K. Sellegri
Project administration: C. S. Law, K. Sellegri
Resources: N. Barr, K. Safi, A. Marriner, J. Uitz, A. Engel, M. J. Harvey, C. S. Law, K. Sellegri
Software: M. Rocco, R. Salignat, J. Uitz
Supervision: E. Dunne, C. S. Law, K. Sellegri
Validation: M. Rocco, E. Dunne, A. Saint-Macary, M. Peltola, T. Barthelmeß, K. Safi, C. Rose, J. Uitz, A. Saiz-Lopez, M. J. Harvey, C. S. Law, K. Sellegri
Visualization: M. Rocco, R. Salignat, A. Saint-Macary, T. Barthelmeß, K. Sellegri
Writing – original draft: M. Rocco
Writing – review & editing: M. Rocco, E. Dunne, R. Salignat, A. Saint-Macary, M. Peltola, T. Barthelmeß, G. Chamba, N. Barr, A. Marriner, S. Deppeler, C. Rose, J. Uitz, J. Harnwell, A. Engel, A. Saiz-Lopez, C. S. Law, K. Sellegri

increased cloud albedo, subsequently cooling Earth's temperature. The proposition of the CLAW hypothesis has been the stimulus for intensive research on the cycle of DMS and its role in atmospheric chemistry and climate processes (Kloster et al., 2006).

In the surface ocean, DMS is produced from the degradation of dimethylsulfoniopropionate (DMSP), which may be produced by marine macroalgae, phytoplankton or bacteria (Bentley & Chasteen, 2004; Kloster et al., 2006; Novak & Bertram, 2020). DMS can also be produced intracellularly by phytoplankton and then directly released into seawater. To form DMS, the DMSP undergoes reactions catalyzed by DMSP lyase (Steinke et al., 1996; Taylor & Visscher, 1996; see Shaw et al., 2022 for a review). Other DMS production pathways have been suggested, including biological catabolism of DMSP and abiotic light-dependent reactions (McNabb & Tortell, 2022 and references therein), but the contribution of these pathways to marine DMS production is still an open question (Shaw et al., 2022). These multiple chemical and biological production pathways make numerical prediction of DMS fluxes complex. Another product of DMSP degradation is methanethiol (MeSH) which is produced from ∼22% of marine DMSP (Kiene, 1996). Although MeSH is more reactive and therefore has a shorter lifetime than DMS in the atmosphere, of a few hours relative to ∼1 day (Lee & Brimblecombe, 2016). Novak et al. (2022) have shown that MeSH is a significant contributor to sulfur emissions, the oxidation of which produces almost exclusively SO_2. However, the role of MeSH in marine aerosol formation is highly uncertain due to the scarcity of data on MeSH emissions, atmospheric concentrations, and photochemical processing. A recent study reported concentrations of MeSH over the Atlantic and Arctic Ocean up to 3.26 ± 1.49 nM (Gros et al., 2023). Other recent studies by Lawson et al. (2020) and Kilgour et al. (2022), concluded that MeSH fluxes are underestimated by a factor of 4 relative to earlier studies by Kettle et al. (2001). However, Novak et al. (2022) showed similar fluxes than Kettle et al. (2001), providing motivation for expanding MeSH observations.

DMS is the main, and often only, compound of marine biogenic origin implemented in regional (Marelle et al., 2017) and global atmospheric models (Carslaw et al., 2013; Mahajan et al., 2015; Woodhouse et al., 2013). However, the role of DMS in climate regulation has been questioned (Quinn & Bates, 2011), and furthermore there is no consensus on the net effect of climate change on DMS emissions within the modeling community. Most studies predict a future increase in global DMS concentrations (Bopp et al., 2004), while other models a decrease under future scenarios (Kloster et al., 2006; Schwinger et al., 2017), with some of this disagreement arising from DMS concentration input to the models. For deriving sea-to-air DMS fluxes, several modeling exercises (e.g., Mahajan et al., 2015; Marelle et al., 2017) use DMS concentration in the seawater derived from bottom-up surface seawater DMS climatologies (Hulswar et al., 2022; Lana et al., 2011). However, these models have limited spatial resolution and also some regions of the globe are poorly documented. Others use the output from ocean biogeochemical models (e.g., Elliott, 2009), in which DMS production is represented by simulating the relationships between different phytoplankton classes with zooplankton, light, temperature and nutrient availability (Vogt et al., 2010), each of which includes some degree of uncertainty.

As ocean biogeochemical models are complex tools, there have been recent attempts to generate DMS fields from a simplified set of biogeochemical parameters. In Wang et al. (2020), a large database of DMS measurements in surface waters was used with a number of environmental parameters to predict oceanic DMS in a neural network approach, but the resulting multi-linear regression only captured ∼30% of the variance in DMS, and also significantly underestimated DMS in regions of high concentrations. Bell et al. (2021) used a set of DMS measurements from four ship campaigns in the North Atlantic to compare the Lana et al. (2011) climatology with the Wang et al. (2020) approach. They reported that the Lana et al. (2011) DMS climatology simulated the seasonal variation of DMS concentration but failed to capture the DMS variability over short spatio-temporal scales. The improved version of the Lana et al. (2011) climatology by Hulswar et al. (2022) used dynamical biogeochemical province boundaries and seasonal changes to significantly improve the estimation of the seawater DMS concentrations and fluxes. Other approaches include Galí et al. (2018), who estimated DMSP from satellite-retrieved Chl-a and light, with sea-surface DMS as a function of DMSP and photosynthetically available radiation (PAR). The Galí et al. (2018) algorithm and neural network model outputs under-predicted measured DMS concentrations in areas such as the Southern Ocean, and it was concluded that this approach was limited by input variables that did not capture all the key biological processes involved in DMS production. In particular, Chl-a may be an inadequate biological variable to predict DMS concentrations, as suggested by many field studies and modeling (Bell et al., 2021; Lana et al., 2011), as it is present in all phytoplankton groups whereas DMS production varies with taxa. Laboratory and mesocosm experiments have shown that DMS is preferentially associated with two phytoplankton groups: dinoflagellates and haptophytes (Kwint et al., 1993; Kwint &

Kramer, 1995; Levasseur et al., 1996; Yassaa et al., 2006), consistent with the elevated cellular DMSP content of these groups (Keller & Korjeff-Bellows, 1996). The haptophyte *Phaeocystis* are major DMS/DMSP producers driving the DMS concentrations in the Southern Ocean (Kim et al., 2017; Stefels et al., 2018). However, the relationship between phylogenetic classes and DMS/DMSP concentrations were not quantified in these studies, and phylogenetic class is not as easily determined as phytoplankton size class that may be measured via satellite approaches (Uitz et al., 2006).

One limitation in relating trace gases to sea-surface biota arises due to spatiotemporal differences arising from atmospheric mixing and transport (Bell et al., 2015). Here, we describe the use of novel deck board Air-Sea Interface Tanks (ASIT), to measure DMS and MeSH fluxes in different seawater types off the south-east of New Zealand in the South-west Pacific. Although the ASITs eliminate wind-induced mixing they enabled direct measurement of DMS and MeSH emissions, and so their respective contribution to total sulphur emissions, as well as determination of their relationship with biogeochemistry of surface waters. These relationships between fluxes and seawater properties were explored in order to develop parameterizations for potential application in modelling. These ASITs provided the capacity to control variables and, as surface ozone has increased in clean Southern Hemisphere air over the last 30 years and projected to continue to increase (Cooper et al., 2020), we also investigated the impact of ozone-mediated oxidative stress on these fluxes.

2. Materials and Methods

The experiments were conducted onboard the *R/V Tangaroa* during the Sea2Cloud voyage in the South-West Pacific Ocean east of New Zealand, around the Chatham Rise (44ºS, 174–181ºE), in the late austral summer from 17 to 27 March 2020 (Sellegri et al., 2023). The Chatham Rise represents the junction where Subantarctic seawater meets Subtropical seawater and supports blooms of high phytoplankton abundance and diversity along the Frontal waters (Law et al., 2017). The Sea2Cloud voyage objectives and measurements are summarized in Sellegri et al. (2023).

2.1. Air-Sea Interaction Tanks (ASITs)

During the Sea2Cloud voyage, two Air-Sea Interface Tanks (ASITs) were deployed for semi-controlled studies of trace gas emission from seawater of differing origin: Subantarctic; Subtropical and Frontal. The ASITs consisted of two cylindrical chambers, each of 1.82 m^3 volume, lined with Teflon film and enclosed by a transparent lid composed of PMMA to minimize loss of short-wave radiation. The water temperature in the ASITs was maintained at ambient surface temperature by a heat exchanger, with water and headspace temperature and light conditions continuously monitored in both tanks (Ecotriplet; HOBO Pendant temp/light, Onset, Bourne MA USA). The ASITs were mounted on the rear deck of the vessel with in-built baffles in each to reduce turbulence and mixing arising from movement of the ship. Ambient air was drawn from above the bridge of the ship via a 400 mm ECOLO Polyurethane Antistatic hose at 1,000 L min^{-1}, a subsample of which was pumped (Gast Manufacturing, MI, USA) via a particle filter through the headspace of each ASIT at ∼23 L min^{-1}, resulting in a residence time of ∼40 min. One ASIT had 7.5 L min^{-1} of the total flushing air enriched to 50 ppbv ozone continuously (ASIT-O_3) using an ozone generator (MGC101, Environmental S.A., Poissy, France), while the other was not modified and so represented a control (ASIT-control). The ozone concentrations in the ambient air, flushing air entering the ASITs and ASIT's headspace are shown in Figure S1 in Supporting Information S1. The ozone concentration in the flushing air is very close to the ambient air concentration, indicating that losses in the 40 m sampling line are limited and that the ozone concentration injected in the ASIT's headspace is representative of the open ocean conditions. The ASIT-control ozone levels measured in the ASIT headspace outlet flow were lower than in ambient air, likely indicative of increased reactivity in the ASITs headspaces relative to ambient air, as biogenic emission fluxes are not ventilated as efficiently as in the ambient air. Losses are also likely due to increased reactivity at the air-sea interface where liquid-phase reactions of ozone with iodine and organic matter were found more effective than in the gas-phase (Hoffmann et al., 2016). We calculated that the total seawater surface losses are of the order of 40% for both the ASIT-control and ASIT-O_3 headspaces. The added ozone in the ASIT-O_3 headspace resulted in an increase of about 10 ppb measured in the ASIT-O_3 headspace outlet, compared to the ASIT-control, and therefore are of a reasonable order of magnitude compared to expected future changes (Cooper et al., 2020). The ASITs experiments, despite the inevitable constraints due to the enclosures themselves, were designed to study natural marine fluxes and open ocean chemistry with natural complexities that can not be achieved in traditional chemistry chamber experiments performed in the laboratory.

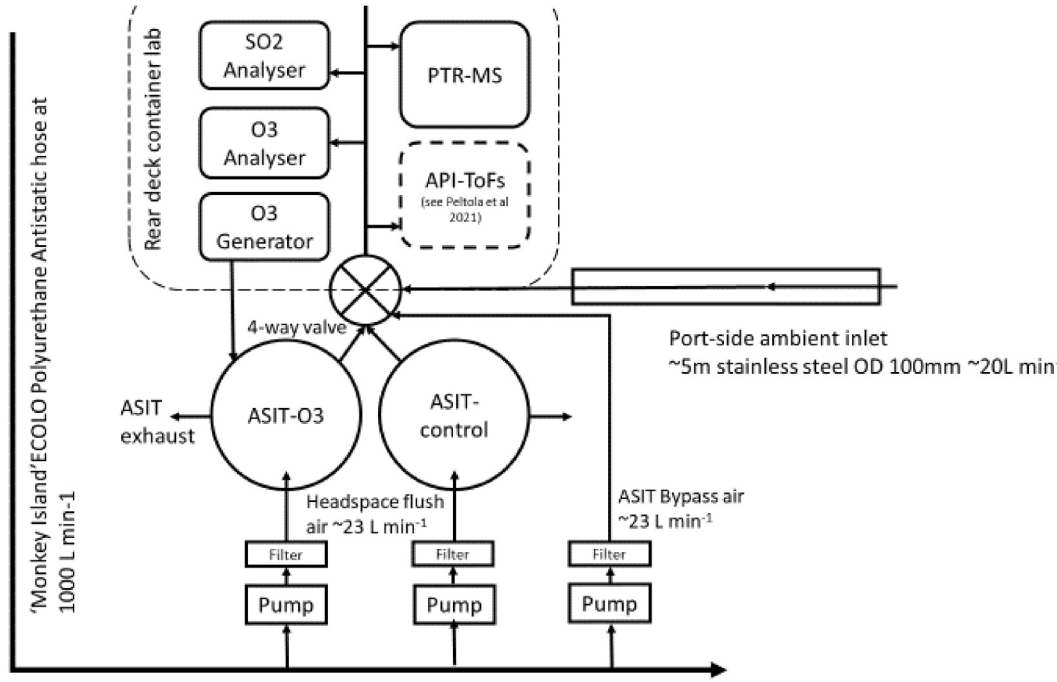

Figure 1. Schematic of the ASITs experimental set-up.

An air-conditioned shipping-container laboratory located on the rear deck adjacent to the ASITs housed a suite of gas and particle monitoring instruments connected to a common sampling manifold (Figure 1). The air being sampled was controlled by a 4-way electronic valve (TSI) that switched every 20 min to sequentially sample: (a) ambient air via an ~5 m stainless steel inlet (OD 100 mm) with the outlet located over the port side of the ship and a flowrate of ~20 L min^{-1}; (b) the ASIT-control, and (c) the ASIT-O_3, each via ~2.14 m of ⅜ inch stainless steel inlets; and (d) the headspace flush air prior to entering the ASITs (ASIT bypass, See Figure 1). Perraud et al. (2016) investigated the losses of MeSH through stainless steel tubes and reported a loss up to 75% when a ~20 cm stainless steel or copper tubing were placed in the sampling line between the certified 4.3 ppm MTO gas cylinder and the PTR-ToF-MS inlet. Our estimation of MeSH is then probably underestimated.

There were variations in the irradiance between the two tanks due to reliance upon natural light on deck. Continuous monitoring of incident PAR showed that cumulative irradiance differed by less than 20% between the two ASITs at the end of the 48-hr experiments for EXP B and C, but was about 40% higher in the ASIT-control compared to ASIT-O_3 during EXP A on the 22nd of March.

2.2. Seawater Sampling and Analysis

At the start of each experiment, the two ASITs were flushed with ambient seawater collected from 3-m depth using a towed fish deployed 3 m from the side whilst the ship was in motion to avoid contamination. Flushing of the ASITs using previously acid-washed piping lasted for 3 hr, after which the two ASITs were filled simultaneously to a volume ~0.9 m^3 and then sealed with ~1 m^3 of headspace air overlying the seawater. Three distinct sea water types were sampled in the individual ASIT experiments (Table S1, Figure 2). Frontal waters were incubated in EXP A for the period 20/03 06:00 LT–22/03 23:00 LT; Subantarctic waters were incubated in EXP B for the period 23/03 06:00 LT–25/03 06:00 LT; and Subtropical water incubated in EXP C for the period 25/03 15:00 LT–27/03 06:00 LT.

Seawater samples were collected from each ASIT at the start of each experiment at 06:00–09:00 and repeated each subsequent day of the experiments, via a gravity-fed outlet pipe, with a total of seven seawater aliquots collected from each ASIT over the course of the three experiments. The daily seawater samples were analyzed for DMS in water (DMS_w) and DMSP concentration (see Saint-Macary et al., 2023 for method), with replicate samples from the two ASITs on day 0 of EXP A agreeing within 6%. Other seawater

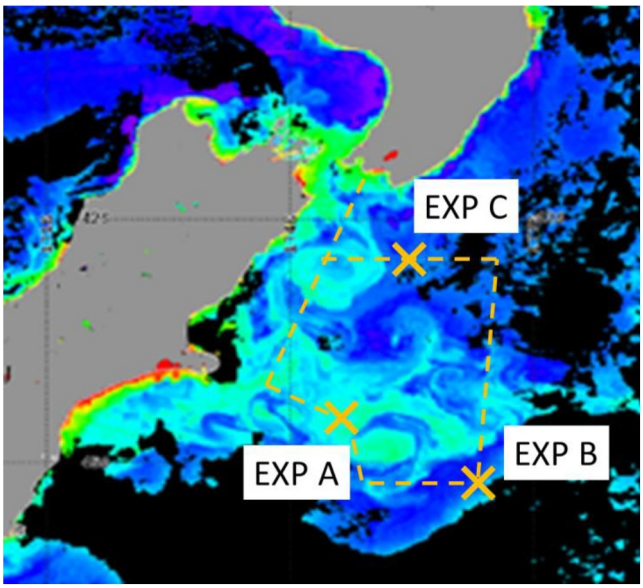

Figure 2. Location of the 3 air-sea interface tanks experiments (EXP A- Frontal water, EXP B - Subantarctic water, EXP C - subtropical water), overlain on a satellite image of ocean color (b_bp443) on 14/3/20, showing the variability and structure of blooms around the Chatham Rise (Image data generated by the Visible Infrared Imaging Radiometer Suite (VIIRS) onboard the Suomi National Polar-orbiting Partnership (SNPP) satellite; data courtesy of NOAA/NESDIS Center for Satellite Applications and Research).

biogeochemical parameters analyzed included Chlorophyll-a (Chl-a), dissolved and particulate nitrogen (DN, PN) and particulate carbon (PC), chromophoric dissolved organic matter (CDOM), total organic carbon, total amino acids (TAA) and combined carbohydrates (TCHO), and also microbial community composition (flow cytometry, flowcam and microscopy). The analysis of the dissolved organic matter components excluded all particles larger than 0.45 µm. Further details of these seawater measurements are provided in Sellegri et al. (2023) and the supplement of this paper. Following each 2-day experiment, the ASITs tanks were drained and cleaned.

2.3. Analysis of ASITs Headspace and Ambient Air

A Proton Transfer Reaction – Quadrupole Mass Spectrometer (PTR-MS, Ionicon Analytik, Innsbruck, Austria) was used to measure VOCs in the ASIT headspace and ambient air. This technique has been described in detail elsewhere (Blake et al., 2009; De Gouw et al., 2003; Lindinger et al., 1998). Briefly, the PTR-MS was operated with an inlet temperature of 60°C, an applied voltage of 600 V and pressure of ~2.0 mbar in the drift tube reaction chamber. The ion source produced H_3O^+ primary reagent ions with a purity of ~97%. The PTR-MS was operated in multiple ion detection mode and scanned 24 selected masses with a 10 s second dwell time. The instrument produced a mass scan every ~3 min. In PTR-MS measurements of the marine atmosphere the ion signals at m/z 49 and m/z 63 are typically attributed to the parent ions of MeSH and DMS (Lawson et al., 2020). Production of other compounds can also contribute to these m/z (Kilgour et al., 2022) but cannot be resolved with the PTR-MS employed in this study.

Zero-air measurements were performed daily by-passing ambient air through a platinum wool catalyst heated to 400°C in order to remove VOCs while maintaining the same mole fractions of the other natural components of air (N_2, O_2, CO_2, H_2O, etc). Zero measurements were conducted separately for each ASIT and for ambient air. The average of these zero measurements was then subtracted from the concentrations obtained in ASIT and ambient VOC measurements. Calibrations were performed with certified gaseous standards (Apel Riemer Env, Inc, Broomfield, CO) containing a mixture of VOCs including ~1 ppm DMS in nitrogen (Stated accuracy ±5%). The PTR-MS sensitivity to DMS was 8.96 ncps/ppbv in ASIT-control and 8.36 ncps/ppbv in ASIT-O_3. No calibration gas for MeSH was available during the voyage. The PTR-MS response to a compound depends on the chemical ionization reaction rate, which is determined by the collision rate constant and the mass-dependent transmission of ions through the mass spectrometer. Due to the similar collision rate constants of MeSH and DMS, and the very similar transmission efficiencies of m/z 63 and m/z 49, we applied the empirically derived PTR-MS response factor for DMS (m/z 63) to the MeSH signal at m/z 49.PTR-MS sensitivities for ambient measurements are 8.47 ncps/ppbv and 4.43 ncps/ppbv for DMS and MeSH, respectively.

The minimum detection limit (MDL) for a single measurement was established by assessing the variability in zero measurements and was defined as the value corresponding to the 95th percentile of the deviations from the mean zero. 100% of the DMS observations collected in the ASITs were greater than the detection limits (MDL (ASIT-control) = 78 pptv, MDL (ASIT-O_3) = 107 pptv). Fourty percent of the observations of MeSH in the ASIT-control were greater than the MDL (15 pptv) and 65% of the observations in the ASIT-O_3 were greater than the MDL (22 pptv). In the ASITs experiments the concentration of DMS and MeSH measured in the bypass air was subtracted from the concentrations measured in the ASITs air in order to quantify the enhancement in DMS and MeSH due to emissions from seawater in the ASITs.

Ozone and sulfur dioxide (SO_2) were continuously measured with a UV photometric analyzer (TEI49i, Thermo Fisher Scientific, Waltham, MA USA) and a SO_2 analyzer using pulsed fluorescence (TEI43i, Thermo Fisher Scientific, Waltham, MA USA). Meteorological parameters experienced during the voyage were measured by an automatic weather station mounted on top of the crow's nest above the bridge.

Contamination of the flushing air from the ship exhaust was filtered out using a SO_2 threshold of 0.2 ppbv; when a spike of SO_2 was observed in the bypass air, data in the ASITs were filtered out from this time on for the following 2 hr 15 min, based on the fact that, at the flow rate of 25 L min^{-1} 90% of the ASITs headspace air is changed in 2 hr 15 min. This time-period was also applied after the lid of the ASITs was closed at the beginning of each experiment with the flux measurements discarded, thus ensuring that the headspace was fully flushed and in equilibrium with the seawater below.

2.4. Headspace-Water Equilibrium in the ASITs

For a given seawater concentration of VOC, the concentration of VOC in the headspace expected at thermodynamic equilibrium can be estimated using the Henry's law equation:

$$\mathrm{VOC}_{\mathrm{air}} = \frac{\mathrm{VOC}_w}{\left(f_{\mathrm{sal}} * H^{cc}_{s(T)}\right)} \tag{1}$$

Where f_{sal} is the factor that accounts for the salinity of seawater ($f_{\mathrm{sal}} = 0.848$ for DMS and 1 for MeSH in the absence of information on this species), experimentally obtained by (Dacey et al., 1984), and $H_s^{cc}(T)$ calculated using the Henry law constant (Sander et al., 2022):

$$H^{cc}_{s(T)} = H^{cp}_{s} \times RT \times \exp\left(B \times \left(\frac{1}{T} - \frac{1}{T_0}\right)\right) \tag{2}$$

where $H_s^{cp} = 5.3 \times 10^{-3}$ mol m^{-3} Pa^{-1} for DMS and $H_0 = 3.8 \times 10^{-3}$ mol m^{-3} Pa^{-1} for MeSH, B is the temperature dependent parameter which is $B = 3500$ K for DMS and $B = 3400$ K for MeSH, R is the molar gas constant $R = 8.314$ J K^{-1} mol^{-1}, T is ambient temperature (in K) and T_0 is reference temperature of 298.15 K. Relatively constant temperatures were maintained during each experiment with minor influence on Henry's law partitioning between aqueous and the gas phase (Rocco et al., 2021; Sinha et al., 2007).

2.5. Determination of Net Fluxes of DMS and MeSH From ASITs Headspace Concentrations

Presuming equilibrium in ASITs, the net fluxes of DMS and MeSH were calculated based on the headspace concentrations measured using PTR-MS, the geometry of ASITs, and the airflow rates in the headspace, as outlined in Equation 3. This methodology has been previously used by Sinha et al. (2007) and detailed in earlier reports from this study (Rocco et al., 2021).

$$F_{\mathrm{VOC}} = \frac{Q}{A} \times \Delta[\mathrm{VOC}]_{\mathrm{ASITs}}(\mathrm{ppb}) \times \frac{M_{\mathrm{VOC}}}{V_m} \tag{3}$$

F_{VOC} is the net flux of VOCs in the ASITs in μg m^{-2} s^{-1}, Q is the flow rate (m^3 s^{-1}) of the bypass air into the mesocosm, A is the surface area of the seawater enclosed in the ASITs in m^2, M_{VOC} is the molecular weight of X compound in kg mol^{-1}, V_m is the molar gas volume in m^3 $kmol^{-1}$ (23.233 at 1015.25 hPa and 283 K) and Δ $[\mathrm{VOC}]_{\mathrm{ASITS}}$ (ppbv) = $[\mathrm{VOC}]_{\mathrm{ASITS}}$ (ppbv) – $[\mathrm{VOC}]_{\mathrm{bypass}}$ (ppbv), where $[\mathrm{VOC}]_{\mathrm{ASITS}}$ (ppbv) is the concentration in the ASITs and $[\mathrm{VOC}]_{\mathrm{bypass}}$ (ppbv) the concentration in the bypass air. The ratios of $[\mathrm{VOC}]_{\mathrm{ASIT}}/[\mathrm{VOC}]_{\mathrm{bypass}}$ ranged from 2.3 to 5.2 across the three experiments.

2.6. Determination of Fluxes of DMS From ASITs Seawater Concentrations

Regional and global models usually calculate fluxes of DMS determined from DMS concentrations in the seawater (e.g., Bopp et al., 2004; Lana et al., 2011; Marelle et al., 2016). Using the measured DMS concentrations in the ASIT seawater, we calculated the DMS fluxes F_c (g cm^{-2} h^{-1}) to the atmosphere following the approach described by Saltzman et al. (1993):

$$Fc = k_{flx}\left(C_l - \frac{C_g}{\alpha}\right) \tag{4}$$

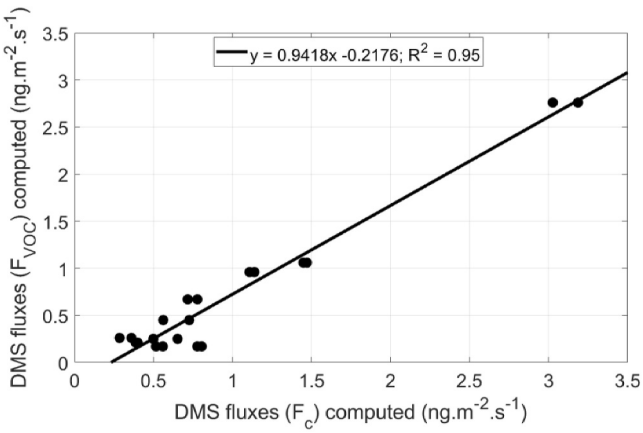

Figure 3. Correlation between dimethyl sulphide (DMS) fluxes computed from Equation 4 (F_c) and using $U = 2.979$ m s^{-1}, for the ASIT-control and $U = 2.419$ m s^{-1} for the ASIT-O_3 and DMS fluxes calculated in both ASITs using Equation 3 (Section 2.5).

where k_{flx} is the gas exchange coefficient, C_g and C_l, the concentrations in the gas and liquid phase, respectively and α is the dimensionless solubility of the gas in the seawater, which is expressed by the McGillis et al. (2000) equation in Equation 5 (C_g is assumed negligible by Marelle et al. (2017)) and k_{flx} by Equation 6 from Wanninkhof (2014):

$$\alpha = e^{\left(\frac{3525}{SST} - 9.464\right)} \quad (5)$$

where SST is the sea surface temperature in K.

$$k_{flx} = 0.251 \left(\frac{660}{S_c(\mathrm{DMS})}\right)^{\frac{1}{2}} u^2 \quad (6)$$

where S_c is the Schmidt number defined by Saltzman et al. (1993):

$$S_c(\mathrm{DMS}) = 2674 - 147.12 \times \mathrm{SST} + 3.726 \times \mathrm{SST}^2 - 0.038 \times \mathrm{SST}^3 \quad (7)$$

in which SST is sea surface temperature in °C and u is wind speed, usually normalized to the height of 10 m above the ocean surface in ambient conditions. We calculated DMS fluxes from the seawater DMS concentrations using the set of equations used in regional modeling, that is, including the wind effect (therefore adding kinetics compared to the Henry's law equilibrium used to plot Figure 6). The measured emission (F_{VOC} in both ASITs, Figure 3) corresponded to calculated DMS fluxes (F_c) for an equivalent wind speed of $U = 2.979$ m s^{-1}, for the ASIT-control and $U = 2.419$ m s^{-1} for the ASIT-O_3, indicating that the measured fluxes in the ASITs were representative of very low wind speed.

2.7. Determination of DMS and MeSH Fluxes From Ambient Marine Boundary Layer Concentrations

For comparison to the ASIT's fluxes, ambient fluxes of DMS and MeSH in the marine boundary layer (MBL) were calculated using the equation described by Marandino et al. (2009) and applied by Lawson et al. (2020) and Rocco et al. (2021):

$$F_{\mathrm{ambientDMS}} = \frac{d[C]}{dt} \times h_{\mathrm{MBL}} \quad (8)$$

Here, $\frac{d[C]}{dt}$ C is the measured DMS concentration in increase over time ng m^{-3}, and h_{MBL} the nocturnal mixed boundary layer in meters determined by radiosonde measurements (ranged between 670 and 1,450 m for the whole campaign). $F_{\mathrm{ambient\ DMS}}$ is the flux of DMS in ambient air in ng m^{-2} s^{-1} deduced from nocturnal DMS measurements. In the same manner as in Marandino et al. (2009) and Lawson et al. (2020), this flux is estimated based on the assumptions of minimal oxidation of DMS during the nighttime and a stable nocturnal mixed boundary layer, which favor the nocturnal accumulation of primary DMS, and a spatial homogeneity in emissions along the air mass back trajectory. Three nights without terrestrial influence were selected for the calculation: from 21 March 21:00 LT to 22 March 06:00 LT, from 22 March 20:00 LT to 23 March 00:00 LT and from 23 March 20:00 LT to 06:00 LT, with corresponding MBL heights of 1,200 m, 670 and 770 m, respectively. Homogeneity of emissions and stable nocturnal mixed boundary layer assumptions were verified by the linear increase in DMS concentrations Figure S2 in Supporting Information S1.

3. Results and Discussion

3.1. Mixing Ratios and Fluxes of DMS and MeSH in the Marine Boundary Layer

Atmospheric mixing ratios of dimethyl sulphide (DMS_a) and methanethiol ($MeSH_a$) sampled via the ambient inlet over the voyage track are shown in Figure 4. Mixing ratios of DMS_a ranged from below detection limit (<78 pptv) to 753 pptv with a voyage average of 171 ± 118 pptv, whereas $MeSH_a$ ranged from below detection limits (<15 pptv) to 150 pptv with a voyage average of 40 ± 28 pptv. The highest concentrations of DMS_a and $MeSH_a$ were

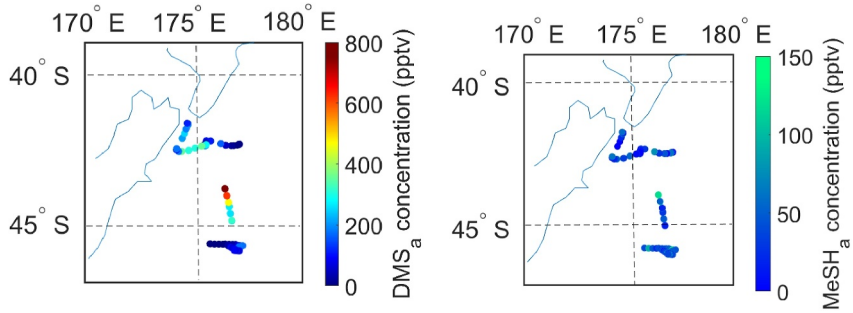

Figure 4. DMS$_a$ and MeSH$_a$ concentrations in the ambient marine boundary layer along the voyage track in pptv.

observed over Frontal waters (Figure 4) and these were similar to that measured during a previous voyage over phytoplankton blooms in this region with a reported DMS$_a$ average of 208 ppt, ranging up to 987 ppt (Bell et al., 2015), and a MeSH$_a$ average of 18 pptv, ranging up to 65 pptv (Lawson et al., 2020). The Lawson et al. maximum was only 44% of the maximum in the current study although this may be due to fewer measurements in the Lawson et al., 2020 study. When both species were detectable the relationship between MeSH$_a$ and DMS$_a$ yielded a slope of 0.13 ($R^2 = 0.52$, Figure 5), which was almost identical to the relationship previously reported by Lawson et al. over a coccolithophore bloom in this region (Slope = 0.13, R^2 = 0.5, Lawson et al., 2020). Furthermore, Novak et al. (2022) showed a similar relationship between MeSH$_a$ and DMS$_a$ than our study and Lawson et al. with slope of 0.19 ($R^2 = 0.61$). The strong correlation between DMS$_a$ and MeSH$_a$ is suggestive of a common seawater source.

The ambient measurements were used to calculate in situ DMS and MeSH fluxes by applying the nocturnal accumulation method (Lawson et al., 2020; Section 2.7) on three separate nights (21–22/03/20 Frontal waters; 22–23/03/24, 23–24/03/24, Subantarctic waters). Calculated emissions were high, ranging between 7.75 and 38.33 ng m^{-2} s^{-1} for DMS and 0.26 and 2.98 ng m^{-2} s^{-1} for MeSH, but in line with values reported in Lawson et al. (2020) where fluxes were 9.1–22.3 ng m^{-2} s^{-1} for DMS and 1.9–3.2 ng m^{-2} s^{-1} for MeSH. The ratio of in situ MeSH:DMS flux was between 0.03 and 0.15, similar to that of Lawson et al. (2020) who obtained a ratio of 0.15 for a phytoplankton bloom. Overall, these studies confirm the biologically productive Subtropical front as a hotspot for sulfur emissions (Lizotte et al., 2017), for both DMS and MeSH. Given the higher reactivity of MeSH with OH, this source could be important for secondary organic aerosol formation and atmospheric oxidation capacity in this region (Novak et al., 2022).

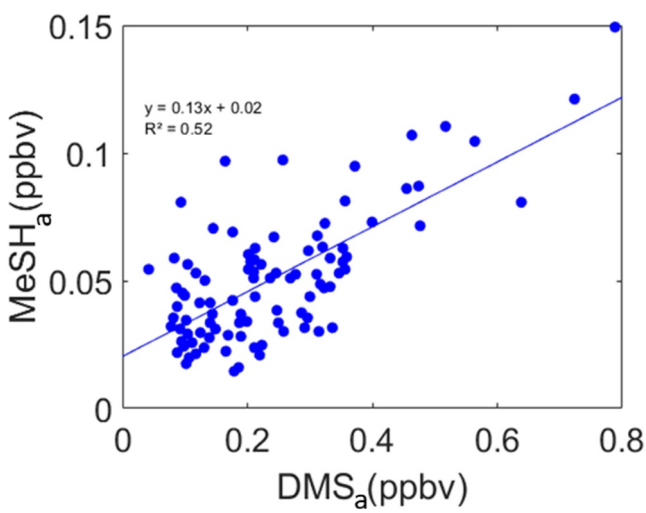

Figure 5. Correlation between ambient DMS$_a$ and MeSH$_a$ concentration (ppbv) in the marine boundary layer.

3.2. DMS and DMSP in the ASITs

The DMS mixing ratio in the headspace was on average one order of magnitude greater in the ASIT-control and 6 times greater in the ASIT-O_3 headspace, relative to the incoming flushing air, indicating that DMS emission from seawater exceeded loss processes in the headspace (e.g., deposition, chemical transformation, wall effects) during the 40 min residence time. Determining DMS air concentration from Henry's law and DMS$_w$ (Equation 1) showed correlation with DMS measured in the headspace (DMS$_{hs}$) (R^2 = 0.88, ρ = 0.61, p_{val} = 0.04, Figure 6), indicating that headspace concentrations are reflecting changes in dissolved DMS concentrations in the underlying seawater. However,the ratio of measured over computed DMS$_{hs}$ (slope = 0.38),indicates that DMS chemical losses are close to 60%, that is, of the same order of as the ozone losses.

In the atmosphere, the lifetime of DMS is estimated to be 16 hr to 1 day if exposed to OH oxidation (Lawson et al., 2020; Lee & Brimblecombe, 2016; Novak et al., 2022), whereas the lifetime of DMS due to ozone oxidation is more than 12 years (calculated from the rate constant value of Burkholder et al. (2015) following Fung et al. (2022)). However modeling studies have shown rapid aqueous phase oxidation of DMS by O_3 (Hoffman et al., 2016)

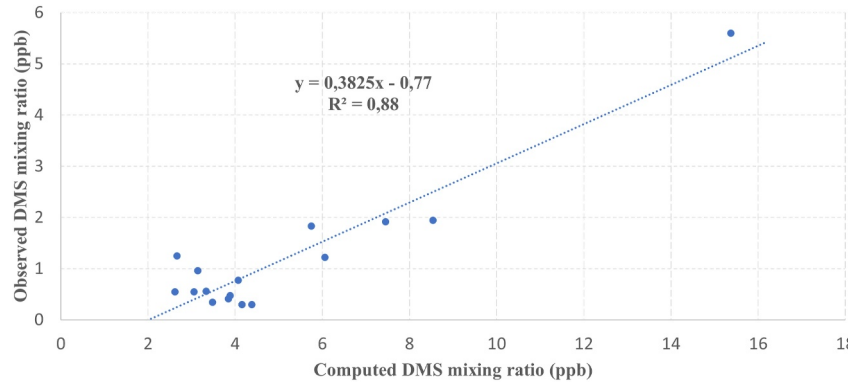

Figure 6. Dimethyl sulphide (DMS) headspace mixing ratios (ppbv) measured in ASITs headspace versus DMS headspace mixing ratios (ppbv) computed from DMS concentrations in the seawater (in nM) using Henry's law.

which may partially explain the lower DMS_{hs} concentrations observed in the ASIT-O_3 compared to the ASIT-control. The DMS_{hs}: DMS_w correlation was similar in the ASIT-control and ASIT-O_3 (slope = 0.51 ± 0.03; intercept = −0.68 ± 0.16; R^2 = 0.97; slope = 0.33 ± 0.04; intercept = −0.32 ± 0.16; R^2 = 0.88, respectively, Figure 7b) indicating that the short residence time (~40 min) limited ozone-driven losses in the ASIT headspace. This is further confirmed by application of Reduced Major Axis regression (Figure S3 in Supporting Information S1).

The highest DMS_{hs} concentrations were observed with Frontal water during EXP A, with maxima of ~6 ppbv in the ASIT-control and ~2.5 ppbv in the ASIT-O_3 (Figure 8 and Figure S3 in Supporting Information S1). Moderate headspace mixing ratios up to 2 ppbv in the ASIT-control and ~1 ppbv in the ASIT-O_3 were observed with Subantarctic water (EXP B), whereas the lowest mixing ratios were obtained with the Subtropical water (EXP C) in both ASIT-control and ASIT-O_3 (~0.5–1 ppbv). In turn, the concentrations of DMS_w were closely related to the concentration of the precursor DMSP (R^2 = 0.69, Figure 7a), with the exception of an outlier DMSP and DMS data point in the ASIT-control at the end of EXP A (Figure 7b).

DMS_w in the ASITs were higher in frontal waters than in the two other water types, with 2.41 ± 1.59 nM, 1.98 ± 0.32 nM and 1.52 ± 0.34 nM in EXP A, B and C, respectively. Concentrations were consistent with concentrations measured in ambient surface seawaters collected at distance from the vessel (5.00 ± 1.75 nM, 2.95 ± 1.77 nM and 1.59 ± 0.16 nM, for Frontal, Subantarctic and Subtropical waters respectively). The higher DMS_w and DMSP concentrations in Frontal waters were consistent with concomitant deck board incubations of sea surface microlayer water, which also showed highest DMS production in Frontal waters at the same location (Saint-Macary et al., 2023). Dissolved DMS concentrations in the Frontal water was lower than previously

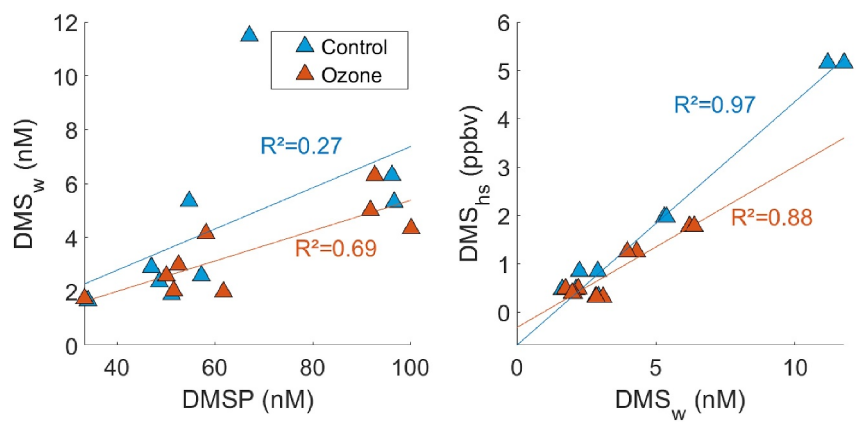

Figure 7. (a) Dissolved dimethyl sulphide (DMS) concentration in the seawater (nM) as a function of DMSP concentrations in the seawater (nM); (b) DMS headspace concentrations as a function of DMS dissolved concentration in the air-sea interface tanks seawater.

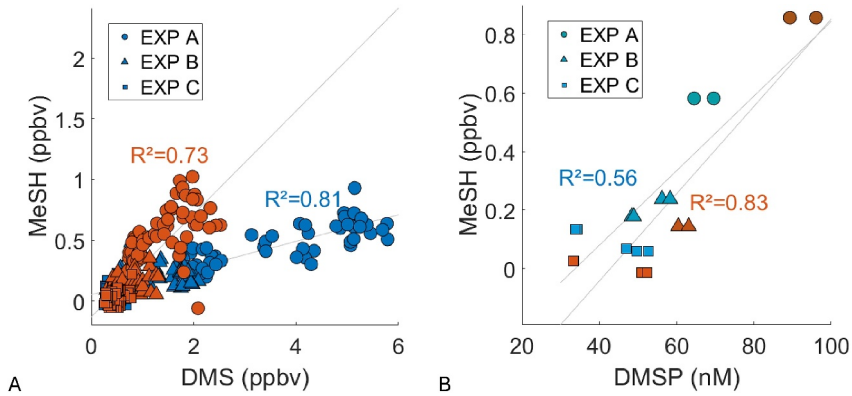

Figure 8. (a) Concentration of $MeSH_{hs}$ versus DMS_{hs} in ppbv. EXP A is represented by circles, B by triangles and C by squares, with the ASIT-control in blue and ASIT-O_3 in orange. R^2(ASIT-control) = 0.73, $p_{value} < 0.001$, $y = 0.11x + 0.05$; r^2(ASIT-O_3) = 0.81, $p_{value} < 0.001$, $y = 0.43x - 0.13$. (b) Concentrations of MeSH (ppbv) versus DMSP concentration (nM) in both ASITs.

reported in Frontal blooms in this region (e.g., 4.9–13.8 nM, Walker et al., 2016), whereas dissolved DMS in the Subantarctic water and Subtropical water samples were similar to those reported in previous studies at Subantarctic and Subtropical latitudes (Dani et al., 2017), indicating the ASITs seawater was broadly representative of water masses in these regions. The concentrations of DMS_w were closely related to the concentration of the precursor DMSP ($R^2 = 0.69$, Figure 7a). Over the course of EXP A DMS_w in the ASIT-control doubled from 5 to 11 nM accompanied by a decrease in DMSP from 94 to 67 nM (Figure S4 in Supporting Information S1). Conversely, only small changes occurred in DMS_w (from 4 to 6 nM) and DMSP (from 100 to 93 nM) in the ASIT-O_3 during EXP A. There were less pronounced anomalies in DMS_w and DMSP (<2 nM DMS_w <5 nM DMSP) between ASIT-control and ASIT-O_3 in EXP B and C (Figure S4 in Supporting Information S1).

The measured DMSP concentrations reported in this work correspond to total DMSP which is comprised of both dissolved and particulate DMSP. Approximately 80% of DMSP is in the particulate form within phytoplankton cells, and so is not available for bacterial catabolism to DMS_w (Belviso et al., 2004; Keller & Korjeff-Bellows, 1996; Yang et al., 2005, until it is released by grazing, viral lysis, or cell lysis during senescence). The role of ozone is unclear, although it may have influenced intracellular DMSP release, potentially inhibiting bacterial/viral lysis of phytoplankton cells toward the end of EXP A. The differential changes in DMS_w and DMSP between ASIT-control and ASIT-O_3 in EXP A (Figure S4 in Supporting Information S1) may also indicate greater catabolism of DMSP to DMS_w in the ASIT-control. This may reflect higher enzymatic cleavage of dissolved DMSP by bacteria and/or lower conversion by demethylation in the ASIT-control (Yoch, 2002). Alternatively, differences between DMS_w and DMSP between ASIT-control and ASIT-O_3 (Figure S5 in Supporting Information S1) may reflect variation in cleavage of intracellular DMSP to DMS by different phytoplankton types (Lizotte et al., 2017), although in our case, the phytoplankton cell abundances did not vary between the ASIT-control and ASIT-O_3 (see Section 3.6) making this hypothesis unlikely. Our results suggest a metabolic influence of ozone; however, recognizing the limited data set and absence of replication in the ASIT experiments, further work is required to confirm this.

3.3. MeSH and Its Relationship to DMS and DMSP

As with DMS, the MeSH atmospheric lifetime (9 hr) is many times greater than the residence time in the ASITs headspace (~40 min) and therefore we assumed that chemical loss processes did not significantly influence MeSH in the experiments. The highest MeSH headspace ($MeSH_{hs}$) concentrations were observed with the Frontal seawater in EXP A, moderate headspace mixing ratios were observed during EXP B with Subantarctic water, and lowest headspace mixing ratios with the Subtropical water in EXP C (Table 1, Figure 8). As $MeSH_w$ was not measured directly, it was calculated from $MeSH_{hs}$ assuming thermodynamic equilibrium according to the Henry's law (Equation 1; Figure S6 in Supporting Information S1), with the relationship between $MeSH_w$ and $MeSH_{hs}$ shown in Figure S7 in Supporting Information S1. Calculated $MeSH_w$ concentrations were 0.26 ± 0.10 nM in the ASIT-control and 0.31 ± 0.14 nM in the ASIT-O_3 for Frontal seawater (EXP A), 0.12 ± 0.05 nM for the ASIT-

Table 1
Spearman Correlations Coefficient (ρ) Between Concentrations of DMS in Headspace (ppb) and Water (nM) and DMSP (nM) and Seawater Biogeochemical Variables Derived From All Samples From the ASIT Experiments

ρ (p_{value})	DMS_{hs} (ppt)	$MeSH_{hs}$ (nM)	DMS_w (nM)	$MeSH_w$ (nM)	DMSP (nM)
Picophytoplankton (cells mL^{-1}) ($n = 16$)	−0.31 (0.12)	**−0.49 (0.05)**	−0.23 (0.19)	−0.33 (0.11)	**−0.47 (0.03)**
Prokaryotic pico - Syne, PrKS (cells mL^{-1}) ($n = 16$)	−0.34 (0.09)	**−0.44 (0.05)**	**−0.55 (0.02)**	**−0.45 (0.04)**	**−0.46 (0.04)**
Nanophytoplankton (cells mL^{-1}) ($n = 16$)	0.36 (0.08)	**0.61 (<0.01)**	**0.76 (<0.01)**	**0.56 (0.02)**	**0.63 (<0.01)**
Dinoflagellates (mgC m^{-3}) ($n = 18$)	0.18 (0.24)	0.35 (0.07)	0.34 (0.08)	0.25 (0.15)	0.21 (0.21)
Diatoms (mgC m^{-3}) ($n = 18$)	0.09 (0.35)	−0.05 (0.42)	0.26 (0.15)	0.09 (0.36)	0.13 (0.31)
Flagellates (mgC m^{-3}) ($n = 18$)	0.21 (0.21)	0.07 (0.39)	**0.44 (0.03)**	0.21 (0.19)	0.12 (0.31)
Bacteria (cells mL^{-1}) ($n = 16$)	0.36 (0.07)	**0.50 (0.02)**	0.32 (0.11)	**0.41 (0.04)**	**0.50 (0.02)**
Chl-a (mg m^{-3}) ($n = 16$)	−0.18 (0.24)	−0.13 (0.29)	0.07 (0.39)	−0.10 (0.34)	0.18 (0.24)
DMS_w (nM) ($n = 18$)	**0.61 (0.04)**	**0.72 (<0.01)**	–	**0.73 (<0.01)**	**0.75 (<0.01)**
$MeSH_w$ (nM) ($n = 18$)	**0.87 (<0.01)**	**0.94 (<0.01)**	**0.73 (<0.01)**	–	**0.75 (<0.01)**
DMSP (nM) ($n = 18$)	**0.55 (0.01)**	**0.72 (<0.01)**	**0.75 (<0.01)**	**0.75 (<0.01)**	–
TOC (μM) SUB ($n = 12$)	0.36 (0.12)	**0.52 (0.04)**	**0.52 (0.04)**	**0.51 (0.05)**	**0.54 (0.04)**
PN (μg N L^{-1}) ($n = 18$)	0.31 (0.10)	**0.52 (0.02)**	**0.65 (0.002)**	**0.52 (0.02)**	**0.59 (<0.01)**
PC (μg C L^{-1}) ($n = 18$)	0.29 (0.12)	**0.49 (0.02)**	**0.58 (0.006)**	**0.48 (0.02)**	**0.54 (0.01)**
TCHO (nmol L^{-1}) ($n = 18$)	0.29 (0.26)	0.39 (0.11)	**0.54 (0.02)**	0.38 (0.12)	**0.60 (<0.01)**
TAA (sum in nmol L^{-1}) ($n = 12$)	**0.76 (<0.01)**	**0.73 (<0.01)**	**0.83 (<0.01)**	**0.78 (<0.01)**	**0.85 (<0.01)**
iodide (nM) ($n = 14$)	**−0.47 (0.05)**	**−0.83 (<0.01)**	**−0.62 (<0.01)**	**−0.64 (<0.01)**	**−0.68 (<0.01)**
iodate (nM) ($n = 14$)	**−0.48 (0.05)**	**−0.87 (<0.01)**	**−0.57 (0.02)**	**−0.73 (<0.01)**	**−0.77 (<0.01)**

Note. Bold values indicate significant correlations ($p_{value} < 0.05$).

control and 0.07 ± 0.05 nM for the ASIT-O_3 for the Subantarctic seawater samples (EXP B) and 0.05 ± 0.03 nM in the ASIT-control and 0.02 ± 0.02 nM in the ASIT-O_3 for the Subtropical seawater (EXP C). The calculated $MeSH_w$ estimates are within the range of concentrations reported in previous studies of ∼0.2 nM in the Baltic Sea (Leck & Rodhe, 1991); 0.4 ± 0.3 nM from the Atlantic Meridional Transect (Kettle et al., 2001); and lower than the reported ∼0.75 nM (up to 3 nM) from the northeast subarctic Pacific Ocean (Kiene et al., 2017), and ∼0.8–3.3 nM in the temperate Atlantic (Gros et al., 2023).

Significant linear Pearson correlations between DMS_{hs} and $MeSH_{hs}$, and also between $MeSH_{hs}$ and DMSP, were found in both ASITs, suggestive of a common production pathway from precursor DMSP (Figure 8a). Conversion to DMS is only a minor (5%–10%) pathway for DMSP removal, which instead occurs predominantly via bacterial demethylation or demethiolation of DMSP to MeSH (Kiene et al., 1999, 2000). However, MeSH is not the only product of DMSP demethylation (Yoch, 2002), it is also rapidly converted to bacterial protein sulfur (Kiene et al., 1999), hence the proportionally higher DMS_{hs} relative to $MeSH_{hs}$. While the slopes of the linear regressions of MeSH/DMS were generally higher for the ASIT-O_3, particularly in EXP A (Figure 8a), the linear regressions of MeSH/DMSP were roughly equivalent between ASIT-control and ASIT-O_3 across the three experiments. Therefore, ozone did not have a detectable influence on the conversion of DMSP to MeSH. Here we note that the correlation of $MeSH_a$ with DMS_a found in the ambient air (Figure 5), shows a similar slope to that observed in the ASIT-control (Figure 8).

3.4. Fluxes of DMS and MeSH in the ASITs

The net fluxes of DMS and MeSH were determined from the headspace data via Equation 3 (Section 2.5, Tables 2 and 3). DMS flux from seawater to headspace was highest with the Frontal water incubation (EXP A: F_{DMS} = 1.44 ± 0.92 ng m^{-2} s^{-1}), moderate fluxes observed with Subantarctic water (EXP B: F_{DMS} = 0.51 ± 0.39 ng m^{-2} s^{-1}) and lowest fluxes from Subtropical water (0.18 ± 0.08 ng m^{-2} s^{-1}) (Figure 9). MeSH fluxes were 6–8 times smaller, but followed the same trends as DMS with fluxes of 0.17 ± 0.06 ng m^{-2} s^{-1} in the Frontal waters, 0.08 ± 0.03 ng m^{-2} s^{-1} with Subantarctic water and 0.04 ± 0.03 ng m^{-2} s^{-1} with

Table 2
Average (±Std. Deviation) of DMS Fluxes in ng m^{-2} s^{-1} for the Three Experiments in the ASITs With Literature Values From the South Pacific Included for Comparison

DMS flux (ng m^{-2} s^{-1})	Seawater origin	Method	Reference
1.44 ± 0.92	Frontal waters	ASIT-Control	This study
0.51 ± 0.39	Subantarctic water		
0.18 ± 0.08	Subtropical water		
0.67 ± 0.26	Frontal waters	ASIT-O_3	
0.22 ± 0.24	Subantarctic water		
0.15 ± 0.07	Subtropical water		
20.5 ± 15.9	South-West Pacific - Chatham Rise (~44°S)	Nocturnal Boundary Layer Accumulation method	This study
9.1 ± 5.3	South-West Pacific - Chatham Rise (~42–46°S)		Lawson et al. (2020)
4.44 ± 1.05	Frontal waters	COARE	Saint-Macary et al. (2023)
2.79 ± 0.83	Subantarctic water		
1.83 ± 0.06	Subtropical water		
2.16 ± 0.46	Mixed waters		
~5.74–7.89	Subantarctic & Antarctic zone (58 and 42°S)	2-layer model	Zhang et al. (2021)
~3.58–5.74	South Subtropical zone (42 and 15°S)		
0.71–61.72	South-West Pacific – Ross Sea (49–76.5°S)	2-layer model	Kiene et al. (2017)
3.1 ± 5.3	Southern Atlantic (~60°S)	2-layer model	Wohl et al. (2020)
2.15–43.1	South-West Pacific - Chatham Rise (~42–46°S)	Eddy Covariance	Bell et al. (2015)

Subtropical water (Table 2). It should be noted that these fluxes estimated using the ASITs are equivalent to very low wind speed (see Section 2.6) and are not representative of the open ocean where elevated wind stress and turbulence will enhance exchange.

As headspace data were mostly collected during nighttime (71%) this limited observations of the influence of PAR on DMS and MeSH production. However, DMS and MeSH fluxes did not correlate with PAR in the three ASITs experiments, with highest PAR during the Subtropical water incubation in EXP C (max 1,600 µmol m^{-2} s^{-1}) which had the lowest DMS and MeSH fluxes ($R^2 < 0.03$, Table S2). Likewise, no correlation was found between the DMS and MeSH fluxes and seawater temperature in the ASITs ($R^2 < 0.05$, Table S2).

Table 3
Average (±Std. Deviation) of MeSH Fluxes in ng m^{-2} s^{-1} for the Three Experiments in the ASITs and Comparison With Literature Values

Average F(MeSH) (ng m^{-2} s^{-1})	Average F(MeSH) % F(DMS + MeSH)	Method/location	Reference
		ASIT-Control	This study
0.17 ± 0.06	11%	Frontal (EXP A)	
0.08 ± 0.03	14%	Subantarctic (EXP B)	
0.04 ± 0.03	18%	Subtropical (EXP C)	
		ASIT-O_3	
0.21 ± 0.09	24%	Frontal (EXP A)	
0.04 ± 0.04	15%	Subantarctic (EXP B)	
0.01 ± 0.02	6%	Subtropical (EXP C)	
1.9 ± 1.4	9%	Nocturnal Accumulation method	This study
2.61 (2.5–4.2)	14%–24%		Lawson et al. (2020)
0.43 (0.21–0.63)	19%	Eddy covariance, North Pacific coastal waters	Novak et al. (2022)
0.09 ± 0.08	6%–7%	Baltic Sea	Leck et al. (1990)
0.66	20%	Atlantic meridional transect	Kettle et al. (2001)

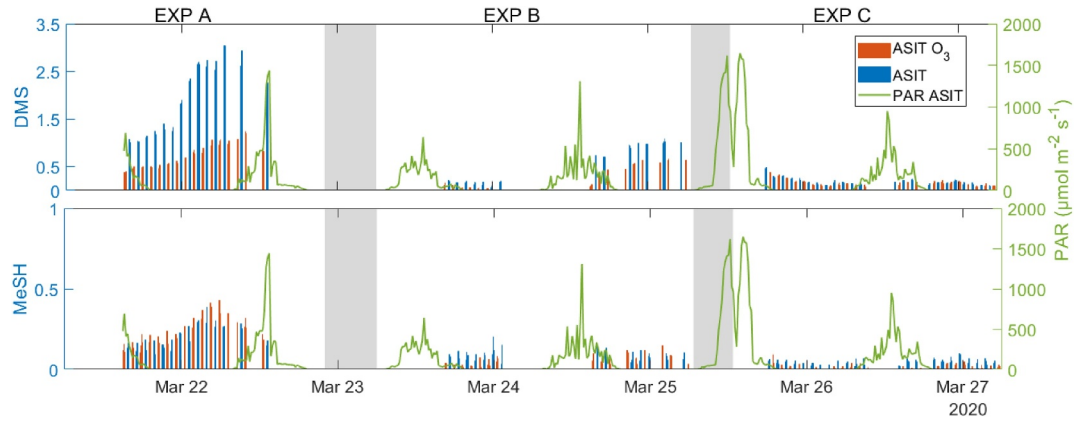

Figure 9. Dimethyl sulphide and MeSH fluxes in ng m^{-2} s^{-1} from air-sea interface tanks (ASIT) control (blue dots) and ozone ASIT (orange dots). Photosynthetically Active Radiation (photosynthetically available radiation, green line) in µmol m^{-2} s^{-1}.

Overall, while irradiance and water temperature may influence fluxes on seasonal or latitudinal scales, changes in these environmental parameters did not appear to be major drivers of fluxes in the ASITs.

3.5. Representativeness of the ASIT Experiments for Open Ocean Processes

DMS fluxes measured in the ASITs and estimated in situ (see Sections 2.6 and 2.7) are reported in Table 2, along with previously reported literature values. Regional in situ fluxes by Saint-Macary et al. (2023) were approximately four times higher than those obtained from the ASITs, which is expected as flux is dependent on wind speed which was excluded in the ASITs. Hulswar et al. (2022) report DMS fluxes of 5–10 µmol m^{-2} d^{-1} for the South-West Pacific region, which corresponds to the higher end of the range reported by Saint-Macary et al. (2023) and are consistent with estimate from the nocturnal boundary layer accumulation method in this study and that of Lawson et al. (2020). Both nocturnal boundary layer accumulation flux estimates are 1–2 orders of magnitude greater than the measured fluxes in the ASIT experiments, again reflecting low turbulence conditions in the ASITs. However, this may also reflect methodological assumptions in the nocturnal boundary layer accumulation flux estimates, which may be biased by long-range transport and vertical dilution which decouples ambient air from the underlying seawater (Bell et al., 2015). In addition to physical factors, seasonal differences in phytoplankton community composition and surface water biogeochemical composition will result in variability in fluxes.

A few studies have reported air-sea fluxes of MeSH, as summarized in Table 3. Fluxes in the Baltic Sea and Atlantic Ocean (Kettle et al., 2001; Leck & Rodhe, 1991) were of the same order of magnitude as the current study. Lawson et al. (2020) reported MeSH flux of 2.61 ng m^{-2} s^{-1} using the nocturnal boundary layer method, which closely agreed with estimates in this study, but exceeded those measured in the ASITs by a factor of 30. Independent to wind speed and turbulence, the percentage ratio of MeSH emission to DMS can be compared between ASITs and free atmosphere. In the ASIT-control, average MeSH fluxes were 11%, 14% and 18% that of DMS (e.g., MeSH/(MeSH + DMS)) in Frontal, Subantarctic and Subtropical ASITs, respectively, consistent with the flux ratios of 9% determined using the nocturnal boundary layer accumulation method in the current study, and also during SOAP (14%–24%, Lawson et al., 2020). Furthermore, the ASIT ratios are within the range of ~5–20% determined in the atmosphere in the northern hemisphere (Gros et al., 2023; Kettle et al., 2001; Kiene et al., 2017; Leck & Rodhe, 1991) and over coastal blooms (Kilgour et al., 2022; Novak et al., 2022). Overall, these combined observations indicate that marine MeSH emissions can significantly contribute to the total marine atmospheric sulfur budget.

3.6. DMS and MeSH Relationships With Biogeochemistry

In parallel to trace gas measurements, we assessed diverse biogeochemical parameters in the seawater of the three ASIT experiments (Table S1, see Sellegri et al., 2023 for methods). Many biogeochemical parameters, including Chl-a, nitrate, phosphate, CDOM, TCHO and TAA exhibited similar or slightly greater concentrations in Frontal waters relative to Subtropical water, with both water types having higher concentrations than Subantarctic water

(see Table S1). Conversely, silicate, iodide and iodate concentrations were lowest in Frontal waters and highest in Subtropical water. These observations are consistent with the general classification of Subantarctic seawater as high nutrient low chlorophyll. These two water masses converge at the front generating elevated phytoplankton biomass (51 mg C m^{-3}) relative to the Subantarctic (12 mg C m^{-3}) and Subtropical (19 mg C m^{-3}). In EXP A (Frontal) and C (Subtropical) the phytoplankton biomass had a greater proportion of nanophytoplankton (2–20 μm), and the phytoplankton community (>5 μm) was comprised of dinoflagellates (~22% of total phytoplankton C biomass) and diatoms (~15% of total phytoplankton C biomass), that were predominantly larger (>20 μm) diatoms of the *Thalassiosira* genus. Slightly higher phytoplankton volume and carbon were observed in the Subtropical seawater in EXP C, which was also dominated by larger (>20 μm) diatoms, including a high proportion of *Guinardia* and *Cylindrotheca* sp. The Subantarctic water in EXP B was characterized by lower phytoplankton volume and carbon, with smaller (10–20 μm) dinoflagellates and diatoms of the *Chaetoceros* genus dominating. Cell abundance of picophytoplankton (<2 μm) and *Synechococcus* showed an inverse relationship to the larger phytoplankton cell size groups, with a minimum in EXP A, and maxima in EXP B and C (see Table S1).

For most paired samples the concentrations of biogeochemical parameters were similar in ASIT-control and ASIT-O_3, and so the data from both ASITs was merged. Spearman rank correlations between DMS and MeSH in water and headspace with bulk seawater biogeochemical properties were determined accordingly (see Table 1). Only weak associations ($\rho < 0.22$, Table 1) were observed between Chl-a and dissolved DMS and MeSH, whereas there were stronger relationships between DMS, DMSP and particularly MeSH with phytoplankton community size and community composition. For example, moderate to strong positive Spearman correlations were observed between nanophytoplankton abundance (cells mL^{-1}) with DMSP, DMS_w and also $MeSH_w$, and reflected in moderate to strong positive correlations between nanophytoplankton abundance with DMS flux and MeSH flux. Moderate positive Spearman correlations were observed between DMSP, DMS_w and $MeSH_w$, with the biomass (mg C m^{-3}) of diatoms, flagellates, and dinoflagellates. Dinoflagellates are high DMSP producers (Keller et al., 1989; Stefels et al., 2007), with some species having the capacity to directly cleave DMSP to DMS (Wolfe & Steinke, 1996). High DMS in Frontal waters in this region was previously associated with dinoflagellates (Walker et al., 2016) and the contemporary study of Saint-Macary et al. (2023) also highlighted the influence of dinoflagellates on DMS and DMSP in the sea surface microlayer. Conversely, large diatoms are considered relatively low DMSP producers, and their dominance in the Subtropical water in EXP C may explain why, despite higher overall phytoplankton Chl-a biomass, the fluxes of DMS and MeSH were relatively low, despite higher overall phytoplankton Chl-a biomass.

DMSP, DMS_w and $MeSH_w$, also showed moderate positive Spearman correlations with bacterial abundance (cells/mL). Bacterial abundance was moderately elevated in the Frontal seawater (5%–20%, see Table S1), which may reflect higher bacterial catabolism of DMSP to DMS and MeSH (Yoch, 2002), although process rate measurements were not made. The DMS_w:DMSP ratio averaged ~0.06 across the three experiments with elevated ratios of 0.17 and 0.09 observed in the ASIT-control on day 2 of EXP A and B, respectively. Previous studies in this region reported DMS_w:DMSP ratios of 0.05–0.07, typical of phytoplankton blooms in which DMS production is dominated by bacterially-mediated pathways, whereas ratios >0.15 associated with large changes in DMS_w are indicative of additional phytoplankton-mediated DMS_w production (Lizotte et al., 2017).

In EXP A and B the net fluxes of DMS and MeSH exhibited a diel pattern with maxima during night-time (Figure 9), followed by a decline over the first few hours after sunrise, which may be attributed to enhanced photochemical removal of DMS and MeSH via reaction with OH during daylight hours. However, this trend would be limited by the 40-min residence time of the ASIT headspace, and the observed consistent relationship between DMS_a and DMS_w suggests photochemical removal was minimal (see Section 3.1). Instead, biological processes may have influenced the diurnal cycling of DMSP, DMS and MeSH. For instance, the production of organic matter in phytoplankton synchronizes with the diel light cycle (Halsey & Jones, 2015), and release may be induced by viral cell lysis or grazing (Aylward et al., 2015, 2017; Biggs et al., 2021), both of which occur at night in surface waters (Horas et al., 2018). As DMSP represents a significant fraction of intracellular organic carbon in phytoplankton (Simó & Dachs, 2002), exudation, viral infection and cell lysis and grazing will result in release (Stefels et al., 2007). As part of the organic matter pool, phytoplankton products including TAA and TCCHO also show a similar release pattern (Moran et al., 2022; Thornton, 2014). DMS and MeSH fluxes were found to be strongly correlated with TAA concentrations ($\rho > 0.73$, Table 1) with MeSH fluxes also correlated with bacterial abundance (Table 1). This implies complex biological interactions linking organic matter release, bacterial consumption and organic matter conversion. Rhodobacterales are common among marine bacteria associated to

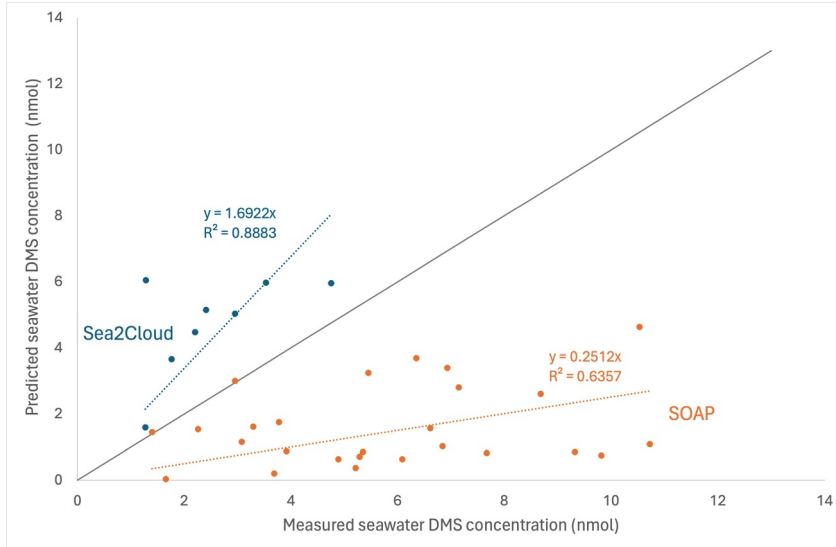

Figure 10. Seawater dimethyl sulphide (DMS) concentrations predicted using Equation 9 and measured nanophytoplankton cell abundances versus measured seawater DMS concentrations for the ambient Sea2Cloud voyage (blue) and the SOAP voyage (orange) excluding an intense dinoflagellate bloom (5 out of 31 data points).

phytoplankton communities and are capable of degrading amino acids and DMSP in comparison to other abundant strains (Ferrer-González et al., 2021). We further note that TCCHO is positively correlated to DMS_w. TCCHO provides structural components or energy to phytoplankton cells and, upon release, support bacterial growth but also aggregate formation. A different effect is seen with iodide and iodate, both anticorrelated to DMS_w and $MeSH_w$. Recent experimental studies concur to show that organics have a suppressive effect on iodide emissions (Schneider et al., 2020; Tinel et al., 2020), even though the underlying mechanisms are not well understood (Tinel et al., 2023). Our results would indicate that DMS and MeSH would have this suppression effect.

3.7. Proxies for Modeling

Sea surface Chl-a concentration is often used as a generic proxy for phytoplankton biomass, and applied in conjunction with other physical and biogeochemical variables in model parameterizations of DMS flux (Aumont et al., 2002; Hulswar et al., 2022; Lana et al., 2011, Simó & Dachs, 2002). However, DMS_w and $MeSH_w$ did not correlate with Chl-a in the ASIT experiments, corroborating the conclusion of many previous studies (Bell et al., 2021; Galí et al., 2018; Kettle et al., 1999; Leck et al., 1990; Simó et al., 1995; Townsend & Keller, 1996), and pointing to the need for a more appropriate biological tracer, particularly over shorter spatiotemporal scales. Most DMS climatologies are derived from data averaged over a large time scale, of the order of the month, thereby smoothing more relevant relationships. We quantified the relationships between measured DMS_w, estimated $MeSH_w$ (see Section 3.3) and the measured nanophytoplankton abundance by using the ASIT control data. This generated the following relationships (Figure S8 in Supporting Information S1):

$$DMS_w\ [\mathrm{nM}] = 3\ 10^{-3}\ [\mathrm{nanophyto, cell/mL}]\ (r = 0.49, p_{\mathrm{value}} < 0.001) \quad (9)$$

$$MeSH_w\ [\mathrm{nM}] = 9.25\ 10^{-5}\ [\mathrm{nanophyto, cell/mL}]\ (r = 0.35, p_{\mathrm{value}} < 0.001) \quad (10)$$

Equation 9 was evaluated on two separate data sets on measured ambient nanophytoplankton cell abundances and seawater DMS concentrations. We used the ambient seawater DMS concentration from the Sea2Cloud voyage, and the data set from the SOAP voyage (Law et al., 2017). The concentrations predicted using Equation 9 are shown against measurements Figure 10. We find that in these two open ocean data sets, the parameterization gives a linear relationship between observed and predicted concentration, but the parameterization overestimates the DMS_w concentrations by a factor ~1.7 for Sea2Cloud and underestimates DMS_w by a factor of ~4 for SOAP. This indicates that other critical factors for predicting DMS abundance are not captured in this empirical relationship.

a)

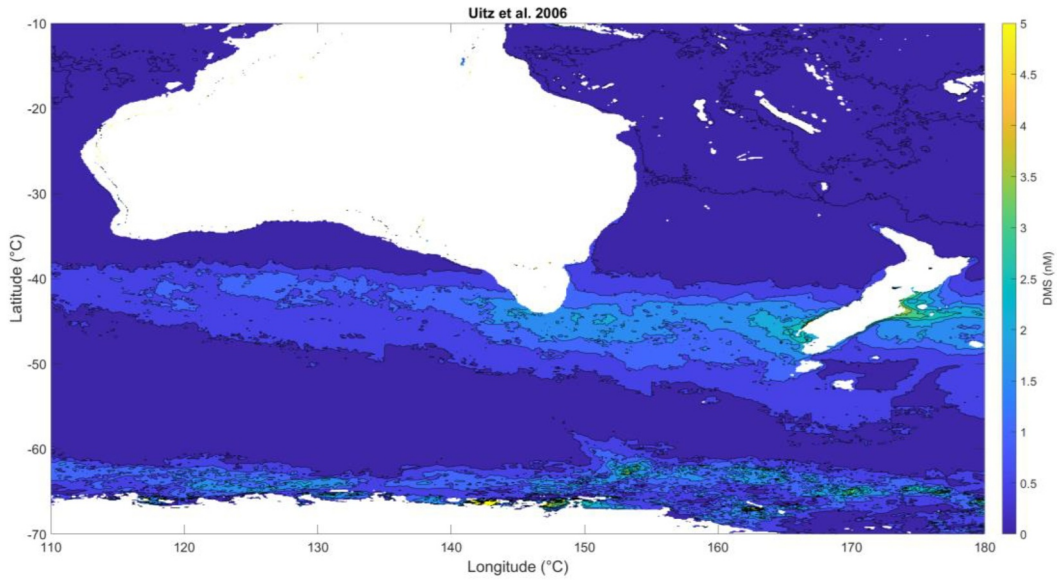

b)

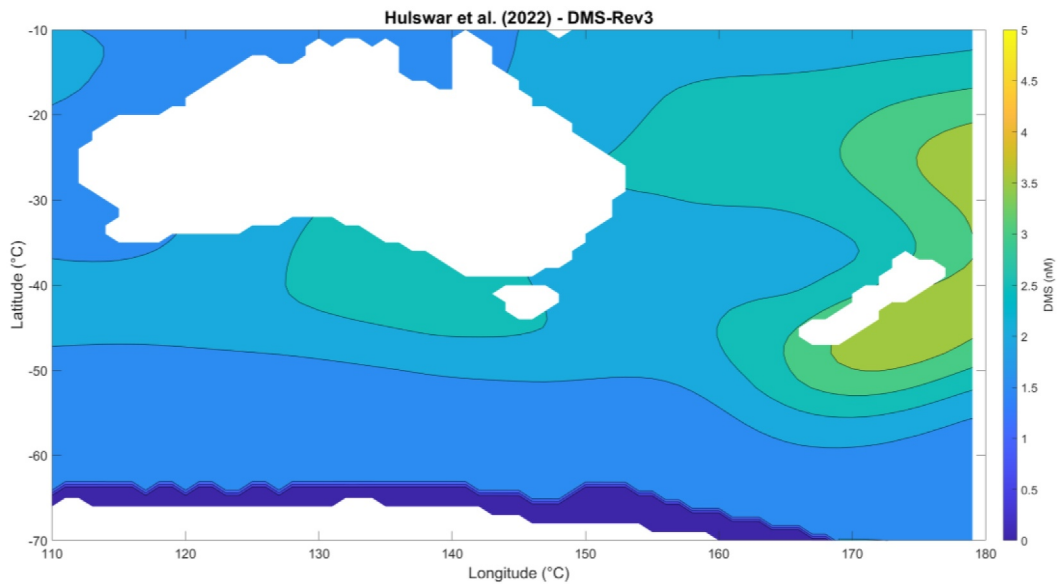

Figure 11. Comparison of the DMS_w concentrations (nM) in March obtained (a) from the combination of Equation 10 and surface nanophytoplankton cell abundances from satellite retrievals according to Uitz et al. (2006) and (b) prognosticated from the climatology of Hulswar et al. (2022).

These relationships may then be tested to predict DMS and MeSH fluxes in regional chemistry transport models as a function of phytoplanktonic size class represented in satellite products (Uitz et al., 2006) or biogeochemical models (Aumont et al., 2015). As nanophytoplankton is defined in terms of carbon biomass in both satellite retrievals and models, in the suggested linear correlations need to be converted to carbon biomass. In the case of satellite retrievals, nanophytoplankton carbon biomass is derived from Chl-a biomass using De Boyer Montégut et al. (2004), whereas for biogeochemical models, the Chl-a m^{-3} in the nanophytoplankton class is parameterized

using a photo-adaptative model in units of mg Chl-a m^{-3} (Geider et al., 1997). Nanophytoplankton Chl-a biomass was converted from MODIS-aqua retrieval and the Uitz et al., 2006 algorithm to cellular abundances (in units of cells mL^{-1}) using an assumed intracellular Chl-a content of 2.64×10^{-10} mg Chl-a $cell^{-1}$ for the nanophytoplankton group (Stramski et al., 2001). For comparison with existing climatologies, DMS_w fields were calculated using Equation 9 with the Uitz et al. (2006) nanophytoplankton surface cell abundances (Sea2Cloud-Uitz), and compared with DMS_w fields extracted from the Hulswar et al. (2021) climatology (Figure 11). The DMS_w fields derived in the present study from the nanophytoplankton satellite retrievals show improved spatial resolution relative to the Hulswar et al., 2022 climatology. For the present study region, the Sea2Cloud-Uitz approach projects DMS_w concentrations ranging from 1 to 4 nM, which are representative of the range of concentrations sampled, while the projection is reduced to 3.2 and 3.6 nM using the Hulswar et al. (2022) climatology. The Sea2Cloud-Uitz approach projects higher DMS_w over two latitudinal zones in the 40°S–50°S and 60°S–70°S range that the Hulswar et al. (2022) climatology does not identify. However, neither our relationship nor the Hulswar climatology have been tested on reliable data in the 60°S–70°S. The prognostic DMS_w range of concentrations derived from the present study is however consistent with the climatology over the large domain shown in Figure 11 (Figure S9b in Supporting Information S1). This gives confidence in applying Equation 10 for testing MeSH fluxes in modeling studies, which, to our knowledge, is not available in current models. Although Equations 9 and 10 have not been tested in other regions, and similar studies are clearly needed, these relationships have potential for investigating how climate change may impact future emissions via its influence on phytoplankton assemblages.

4. Conclusion

Fluxes of MeSH and DMS were determined in deckboard incubations of seawater collected around the Frontal zone in the Southwest Pacific as part of the Sea2Cloud campaign. Seawaters of Frontal, Subantarctic and Subtropical waters were sampled, with paired experiments conducted with differing headspace ozone concentrations. Good agreement was observed between DMS in the headspace and dissolved DMS in the sampled seawater in line with that expected from thermodynamic equilibrium. The MeSH:DMS flux ratio was 11%–18% across the three water mass types, confirming that MeSH may represent a significant unaccounted contribution to the atmospheric sulfur budget, with potentially important implications for marine aerosol formation and growth in models. Elevated ozone resulted in a ∼50% decrease in DMS flux in the Subantarctic and Frontal water incubations, which coincided with a lower DMS:DMSP ratio in the seawater, whereas there was no significant effect of ozone on the MeSH:DMSP ratio. The experimental set-up in our study provided a new approach to relating DMS and MeSH fluxes to the biogeochemical properties of surface seawater. Previous empirical relationships linking DMS fluxes and seawater biology have used Chl-a derived from satellite retrievals, which have inherent spatial resolution and biological limitations. Fluxes of DMS and MeSH concentrations in the seawater showed a significant relationship with nanophytoplankton cell abundance, and this was used to generate parameterizations for dissolved DMS and MeSH. Recent decades have seen an expansion in the use of more sophisticated bio-optical remote sensing products that can extract information on phytoplankton functional types, size classes and taxonomic composition (e.g., Alvain et al., 2005; Gantt et al., 2009); these may be combined with the derived relationships to constrain regional estimates of dissolved DMS and MeSH. From these estimates, DMS and MeSH fluxes may be calculated by using models such as COARE for DMS or thermodynamic and kinetic empirical relationships for both DMS and MeSH.

Data Availability Statement

Data sets reported in this manuscript are available at the Sea2Cloud project data repository at https://sea2cloud.data-terra.org/en/catalogue/ or Catalogue–aeris (aeris-data.fr).

Acknowledgments
This research received funding from the European Research Council (ERC) under the Horizon 2020 research and innovation programme (Grant 771369) and was supported by New Zealand Scientific Strategic Funding via the NIWA Climate, Atmosphere and Hazards Centre. Sea2Cloud is endorsed by SOLAS.

References

Alvain, S., Moulin, C., Dandonneau, Y., & Breon, F. M. (2005). Remote sensing of phytoplankton groups in case 1 waters from global SeaWiFS imagery. *Deep Sea Research Part I: Oceanographic Research Papers*, *52*(11), 1989–2004. https://doi.org/10.1016/J.DSR.2005.06.015

Aumont, O., Belviso, S., & Monfray, P. (2002). Dimethylsulfoniopropionate (DMSP) and dimethylsulfide (DMS) sea surface distributions simulated from a global three-dimensional ocean carbon cycle model. *Journal of Geophysical Research: Oceans*, *107*(C4), 4-1. https://doi.org/10.1029/1999JC000111

Aumont, O., Éthé, C., Tagliabue, A., Bopp, L., & Gehlen, M. (2015). PISCES-v2: An ocean biogeochemical model for carbon and ecosystem studies. *Geoscientific Model Development Discussions*, *8*(2), 1375–1509. https://doi.org/10.5194/gmd-8-2465-2015

Aylward, F. O., Boeuf, D., Mende, D. R., Wood-Charlson, E. M., Vislova, A., Eppley, J. M., et al. (2017). Diel cycling and long-term persistence of viruses in the ocean's euphotic zone. *Proceedings of the National Academy of Sciences*, *114*(43), 11446–11451. https://doi.org/10.1073/pnas.1714821114

Aylward, F. O., Eppley, J. M., Smith, J. M., Chavez, F. P., Scholin, C. A., & DeLong, E. F. (2015). Microbial community transcriptional networks are conserved in three domains at ocean basin scales. *Proceedings of the National Academy of Sciences*, *112*(17), 5443–5448. https://doi.org/10.1073/pnas.1502883112

Bell, T. G., De Bruyn, W., Marandino, C. A., Miller, S. D., Law, C. S., Smith, M. J., & Saltzman, E. S. (2015). Dimethylsulfide gas transfer coefficients from algal blooms in the Southern Ocean. *Atmospheric Chemistry and Physics*, *15*(4), 1783–1794. https://doi.org/10.5194/acp-15-1783-2015

Bell, T. G., Porter, J. G., Wang, W. L., Lawler, M. J., Boss, E., Behrenfeld, M. J., & Saltzman, E. S. (2021). Predictability of seawater DMS during the North Atlantic aerosol and marine ecosystem study (NAAMES). *Frontiers in Marine Science*, *7*, 596763. https://doi.org/10.3389/FMARS.2020.596763/BIBTEX

Belviso, S., Moulin, C., Bopp, L., & Stefels, J. (2004). Assessment of a global climatology of oceanic dimethylsulfide (DMS) concentrations based on SeaWiFS imagery (1998-2001). *Canadian Journal of Fisheries and Aquatic Sciences*, *61*(5), 804–816. https://doi.org/10.1139/f04-001

Bentley, R., & Chasteen, T. G. (2004). Environmental VOSCs—formation and degradation of dimethyl sulfide, methanethiol and related materials. *Chemosphere*, *55*(3), 291–317. https://doi.org/10.1016/J.CHEMOSPHERE.2003.12.017

Biggs, T. E., Huisman, J., & Brussaard, C. P. (2021). Viral lysis modifies seasonal phytoplankton dynamics and carbon flow in the Southern Ocean. *The ISME Journal*, *15*(12), 3615–3622. https://doi.org/10.1038/s41396-021-01033-6

Blake, R. S., Monks, P. S., & Ellis, A. M. (2009). Proton-transfer reaction mass spectrometry. *Chemical Reviews*, *109*(3), 861–896. https://doi.org/10.1021/CR800364Q/ASSET/IMAGES/MEDIUM/CR-2008-00364Q_0003.GIF

Bopp, L., Boucher, O., Aumont, O., Belviso, S., Dufresne, J. L., Pham, M., & Monfray, P. (2004). Will marine dimethylsulfide emissions amplify or alleviate global warming? A model study. *Canadian Journal of Fisheries and Aquatic Sciences*, *61*(5), 826–835. https://doi.org/10.1139/f04-045

Burkholder, J. B., Sander, S. P., Abbatt, J. P. D., Barker, J. R., Huie, R. E., Kolb, C. E., et al. (2015). *Chemical kinetics and photochemical data for use in atmospheric studies: Evaluation number 18*. Jet Propulsion Laboratory, National Aeronautics and Space Administration.

Carslaw, K. S., Lee, L. A., Reddington, C. L., Pringle, K. J., Rap, A., Forster, P. M., et al. (2013). Large contribution of natural aerosols to uncertainty in indirect forcing. *Nature*, *503*(7474), 67–71. https://doi.org/10.1038/nature12674

Charlson, R. J., Lovelock, J. E., Andreae, M. O., & Warren, S. G. (1987). Oceanic phytoplankton, atmospheric sulphur, cloud albedo and climate. *Nature*, *326*(6114), 655–661. https://doi.org/10.1038/326655a0

Cooper, O. R., Schultz, M. G., Schröder, S., Chang, K. L., Gaudel, A., Benítez, G. C., et al. (2020). Multi-decadal surface ozone trends at globally distributed remote locations. *Elem Sci Anth*, *8*, 23. https://doi.org/10.1525/ELEMENTA.420/112772

Dacey, W. H. J., Wakeham, G. S., & Howes, L. B. (1984). Henry's law constants for dimethylsulfide in freshwater and seawater. *Geophysical Research Letters*, *11*(10), 991–994. https://doi.org/10.1029/GL011i010p00991

Dani, K. S., Benavides, A. M. S., Michelozzi, M., Peluso, G., Torzillo, G., & Loreto, F. (2017). Relationship between isoprene emission and photosynthesis in diatoms, and its implications for global marine isoprene estimates. *Marine Chemistry*, *189*, 17–24. https://doi.org/10.1016/j.marchem.2016.12.005

de Boyer Montégut, C., Madec, G., Fischer, A. S., Lazar, A., & Iudicone, D. (2004). Mixed layer depth over the global ocean: An examination of profile data and a profile-based climatology. *Journal of Geophysical Research*, *109*(C12). https://doi.org/10.1029/2004jc002378

De Gouw, J. A., Goldan, P. D., Warneke, C., Kuster, W. C., Roberts, J. M., Marchewka, M., et al. (2003). Validation of proton transfer reaction-mass spectrometry (PTR-MS) measurements of gas-phase organic compounds in the atmosphere during the New England Air Quality Study (NEAQS) in 2002. *Journal of Geophysical Research*, *108*(D21). https://doi.org/10.1029/2003JD003863

Elliott, S. (2009). Dependence of DMS global sea-air flux distribution on transfer velocity and concentration field type. *Journal of Geophysical Research*, *114*(G2). https://doi.org/10.1029/2008JG000710

Ferrer-González, F. X., Widner, B., Holderman, N. R., Glushka, J., Edison, A. S., Kujawinski, E. B., & Moran, M. A. (2021). Resource partitioning of phytoplankton metabolites that support bacterial heterotrophy. *The ISME Journal*, *15*(3), 762–773. https://doi.org/10.1038/s41396-020-00811-y

Fung, K. M., Heald, C. L., Kroll, J. H., Wang, S., Jo, D. S., Gettelman, A., et al. (2022). Exploring dimethyl sulfide (DMS) oxidation and implications for global aerosol radiative forcing. *Atmospheric Chemistry and Physics*, *22*(2), 1549–1573. https://doi.org/10.5194/acp-22-1549-2022

Galí, M., Levasseur, M., Devred, E., Simó, R., & Babin, M. (2018). Sea-surface dimethylsulfide (DMS) concentration from satellite data at global and regional scales. *Biogeosciences*, *15*(11), 3497–3519. https://doi.org/10.5194/bg-15-3497-2018

Gantt, B., Meskhidze, N., & Kamykowski, D. J. A. C. (2009). A new physically-based quantification of marine isoprene and primary organic aerosol emissions. *Atmospheric Chemistry and Physics*, *9*(14), 4915–4927. https://doi.org/10.5194/ACP-9-4915-2009

Geider, R. J., MacIntyre, H. L., & Kana, T. M. (1997). Dynamic model of phytoplankton growth and acclimation: Responses of the balanced growth rate and the chlorophyll a: Carbon ratio to light, nutrient-limitation and temperature. *Marine Ecology Progress Series*, *148*, 187–200. https://doi.org/10.3354/meps148187

Gros, V., Bonsang, B., Sarda-Estève, R., Nikolopoulos, A., Metfies, K., Wietz, M., & Peeken, I. (2023). Concentrations of dissolved dimethyl sulfide (DMS), methanethiol and other trace gases in context of microbial communities from the temperate Atlantic to the Arctic Ocean. *Biogeosciences*, *20*(4), 851–867. https://doi.org/10.5194/BG-20-851-2023

Halsey, K. H., & Jones, B. M. (2015). Phytoplankton strategies for photosynthetic energy allocation. *Annual Review of Marine Science*, *7*(1), 265–297. https://doi.org/10.1146/annurev-marine-010814-015813

Hoffmann, E. H., Tilgner, A., Schroedner, R., Bräuer, P., Wolke, R., & Herrmann, H. (2016). An advanced modeling study on the impacts and atmospheric implications of multiphase dimethyl sulfide chemistry. *Proceedings of the National Academy of Sciences*, *113*(42), 11776–11781. https://doi.org/10.1073/pnas.1606320113

Horas, E. L., Theodosiou, L., & Becks, L. (2018). Why are algal viruses not always successful? *Viruses*, *10*(9), 474. https://doi.org/10.3390/v10090474

Hulswar, S., Simó, R., Galí, M., Bell, T., Lana, A., Inamdar, S., & Mahajan, A. S. (2021). Third revision of the global surface seawater dimethyl sulfide climatology (DMS-Rev3). *Earth System Science Data Discussions*, *2021*, 1–56.

Hulswar, S., Simó, R., Galí, M., Bell, T. G., Lana, A., Inamdar, S., et al. (2022). Third revision of the global surface seawater dimethyl sulfide climatology (DMS-Rev3). *Earth System Science Data*, *14*(7), 2963–2987. https://doi.org/10.5194/essd-14-2963-2022

Keller, M. D., Bellows, W. K., & Guillard, R. R. (1989). Dimethyl sulfide production in marine phytoplankton. *ACS Symposium Series*, 167–182. https://doi.org/10.1021/bk-1989-0393.ch011

Keller, M. D., & Korjeff-Bellows, W. (1996). Physiological aspects of the production of dimeyhtlsulfoniopropionate (DMSP) by marine phytoplankton. In *Biological and environmental chemistry of DMSP and related sulfonium compounds* (pp. 131–142). Springer US. https://doi.org/10.1007/978-1-4613-0377-0_12

Kettle, A. J., Andreae, M. O., Amouroux, D., Andreae, T. W., Bates, T. S., Berresheim, H., et al. (1999). A global database of sea surface dimethylsulfide (DMS) measurements and a procedure to predict sea surface DMS as a function of latitude, longitude, and month. *Global Biogeochemical Cycles*, *13*(2), 399–444. https://doi.org/10.1029/1999GB900004

Kettle, A. J., Rhee, T. S., Von Hobe, M., Poulton, A., Aiken, J., & Andreae, M. O. (2001). Assessing the flux of different volatile sulphur gases from the ocean to the atmosphere. *Journal of Geophysical Research*, *106*(D11), 12193–12209. https://doi.org/10.1029/2000JD900630

Kiene, R. P. (1996). Production of methanethiol from dimethylsulfoniopropionate in marine surface waters. *Marine Chemistry*, *54*(1–2), 69–83. https://doi.org/10.1016/0304-4203(96)00006-0

Kiene, R. P., Linn, L. J., & Bruton, J. A. (2000). New and important roles for DMSP in marine microbial communities. *Journal of Sea Research*, *43*(3–4), 209–224. https://doi.org/10.1016/S1385-1101(00)00023-X

Kiene, R. P., Linn, L. J., González, J., Moran, M. A., & Bruton, J. A. (1999). Dimethylsulfoniopropionate and methanethiol are important precursors of methionine and protein-sulphur in marine bacterioplankton. *Applied and Environmental Microbiology*, *65*(10), 4549–4558. https://doi.org/10.1128/AEM.65.10.4549-4558.1999/ASSET/9D051A80-F6E1-4C7C-8186-D16A8B1AD98A/ASSETS/GRAPHIC/AM1090897008.JPEG

Kiene, R. P., Williams, T. E., Esson, K., Tortell, P. D., & Dacey, J. W. H. (2017). *Methanethiol concentrations and Sea-Air fluxes in the subarctic NE Pacific Ocean*. AGUFM. OS21A-1356. https://ui.adsabs.harvard.edu/abs/2017AGUFMOS21A1356K/abstract

Kilgour, D. B., Novak, G. A., Sauer, J. S., Moore, A. N., Dinasquet, J., Amiri, S., et al. (2022). Marine gas-phase sulphur emissions during an induced phytoplankton bloom. *Atmospheric Chemistry and Physics*, *22*(2), 1601–1613. https://doi.org/10.5194/ACP-22-1601-2022

Kim, I., Hahm, D., Park, K., Lee, Y., Choi, J.-O., Zhang, M., et al. (2017). Characteristics of the horizontal and vertical distributions of dimethyl sulfide throughout the Amundsen Sea Polynya. *Science of the Total Environment*, *584–585*, 154–163. https://doi.org/10.1016/j.scitotenv.2017.01.165

Kloster, S., Feichter, J., Maier-Reimer, E., Six, K. D., Stier, P., & Wetzel, P. (2006). DMS cycle in the marine ocean-atmosphere system - A global model study. *Biogeosciences*, *3*(1), 29–51. https://doi.org/10.5194/BG-3-29-2006

Korhonen, H., Carslaw, K. S., Spracklen, D. V., Mann, G. W., & Woodhouse, M. T. (2008). Influence of oceanic dimethyl sulfide emissions on cloud condensation nuclei concentrations and seasonality over the remote southern hemisphere oceans: A global model study. *Journal of Geophysical Research*, *113*(D15). https://doi.org/10.1029/2007JD009718

Kwint, R. L., & Kramer, K. J. (1995). Dimethylsulphide production by Plankton communities. *Marine Ecology Progress Series*, *121*(1–3), 227–237. https://doi.org/10.3354/MEPS121227

Kwint, R. L., Kramer, K. J., Baart, A. C., & Verhagen, H. L. (1993). The production of DMS by a plankton community-a mesocosm experiment. In *International symposium on dimethylsulphide: Oceans, atmosphere and climate* (pp. 53–62). Kluwer Academic Publishers.

Lana, A., Bell, T. G., Simó, R., Vallina, S. M., Ballabrera-Poy, J., Kettle, A. J., et al. (2011). An updated climatology of surface dimethlysulfide concentrations and emission fluxes in the global ocean. *Global Biogeochemical Cycles*, *25*(1), 1004. https://doi.org/10.1029/2010GB003850

Law, C. S., Smith, M. J., Harvey, M. J., Bell, T. G., Cravigan, L. T., Elliott, F. C., et al. (2017). Overview and preliminary results of the surface ocean aerosol production (SOAP) campaign. *Atmospheric Chemistry and Physics*, *17*(22), 13645–13667. https://doi.org/10.5194/ACP-17-13645-2017

Lawson, S. J., Law, C. S., Harvey, M. J., Bell, T. G., Walker, C. F., De Bruyn, W. J., & Saltzman, E. S. (2020). Methanethiol, dimethyl sulfide and acetone over biologically productive waters in the Southwest Pacific ocean. *Atmospheric Chemistry and Physics*, *20*(5), 3061–3078. https://doi.org/10.5194/ACP-20-3061-2020

Leck, C., Larsson, U., Bågander, L. E., Johansson, S., & Hajdu, S. (1990). Dimethyl sulfide in the Baltic Sea: Annual variability in relation to biological activity. *Journal of Geophysical Research*, *95*(C3), 3353–3363. https://doi.org/10.1029/JC095IC03P03353

Leck, C., & Rodhe, H. (1991). Emissions of marine biogenic sulphur to the atmosphere of northern Europe. *Journal of Atmospheric Chemistry*, *12*(1), 63–86. https://doi.org/10.1007/BF00053934/METRICS

Lee, C. L., & Brimblecombe, P. (2016). Anthropogenic contributions to global Carbonyl sulfide, carbon Disulfide and Organosulfides fluxes. *Earth-Science Reviews*, *160*, 1–18. https://doi.org/10.1016/J.EARSCIREV.2016.06.005

Levasseur, M., Michaud, S., Egge, J., Cantin, G., Nejstgaard, J. C., Sanders, R., et al. (1996). Production of DMSP and DMS during a mesocosm study of an Emiliania Huxleyi bloom: Influence of bacteria and Calanus Finmarchicus grazing. *Marine Biology*, *126*(4), 609–618. https://doi.org/10.1007/BF00351328/METRICS

Lindinger, W., Hansel, A., & Jordan, A. (1998). On-line monitoring of volatile organic compounds at Pptv levels by means of proton-transfer-reaction mass spectrometry (PTR-MS) Medical applications, Food control and environmental research. *International Journal of Mass Spectrometry and Ion Processes*, *173*(3), 191–241. https://doi.org/10.1016/S0168-1176(97)00281-4

Lizotte, M., Levasseur, M., Law, C. S., Walker, C. F., Safi, K. A., Marriner, A., & Kiene, R. P. (2017). Dimethylsulfoniopropionate (DMSP) and dimethyl sulfide (DMS) cycling across contrasting biological hotspots of the New Zealand subtropical front. *Ocean Science*, *13*(6), 961–982. https://doi.org/10.5194/OS-13-961-2017

Mahajan, A. S., Fadnavis, S., Thomas, M. A., Pozzoli, L., Gupta, S., Royer, S. J., et al. (2015). Quantifying the impacts of an updated global dimethyl sulfide climatology on cloud microphysics and aerosol radiative forcing. *Journal of Geophysical Research: Atmospheres*, *120*(6), 2524–2536. https://doi.org/10.1002/2014JD022687

Marandino, C. A., De Bruyn, W. J., Miller, S. D., & Saltzman, E. S. (2009). Open Ocean DMS air/sea fluxes over the eastern south Pacific Ocean. *Atmospheric Chemistry and Physics*, *9*(2), 345–356. https://doi.org/10.5194/ACP-9-345-2009

Marelle, L., Raut, J. C., Law, K. S., Berg, L. K., Fast, J. D., Easter, R. C., et al. (2017). Improvements to the WRF-Chem 3.5. 1 model for quasi-hemispheric simulations of aerosols and ozone in the Arctic. *Geoscientific Model Development*, *10*(10), 3661–3677. https://doi.org/10.5194/GMD-10-3661-2017

Marelle, L., Thomas, J. L., Raut, J. C., Law, K. S., Jalkanen, J. P., Johansson, L., et al. (2016). Air quality and radiative impacts of Arctic shipping emissions in the summertime in northern Norway: From the local to the regional scale. *Atmospheric Chemistry and Physics*, *16*(4), 2359–2379. https://doi.org/10.5194/ACP-16-2359-2016

McGillis, W. R., Dacey, J. W. H., Frew, N. M., Bock, E. J., & Nelson, R. K. (2000). Water-air flux of dimethylsulfide. *Journal of Geophysical Research*, *105*(C1), 1187–1193. https://doi.org/10.1029/1999JC900243

McNabb, B. J., & Tortell, P. D. (2022). Improved prediction of dimethyl sulfide (DMS) distributions in the northeast subarctic Pacific using machine-learning algorithms. *Biogeosciences*, *19*(6), 1705–1721. https://doi.org/10.5194/BG-19-1705-2022

Moran, M. A., Kujawinski, E. B., Schroer, W. F., Amin, S. A., Bates, N. R., Bertrand, E. M., et al. (2022). Microbial metabolites in the marine carbon cycle. *Nature microbiology*, *7*(4), 508–523. https://doi.org/10.1038/s41564-022-01090-3

Novak, G. A., & Bertram, T. H. (2020). Reactive VOC production from photochemical and heterogeneous reactions occurring at the air-ocean interface. *Accounts of Chemical Research*, *53*(5), 1014–1023. https://doi.org/10.1021/ACS.ACCOUNTS.0C00095/ASSET/IMAGES/LARGE/AR0C00095_0004.JPEG

Novak, G. A., Kilgour, D. B., Jernigan, C. M., Vermeuel, M. P., & Bertram, T. H. (2022). Oceanic emissions of dimethyl sulfide and methanethiol and their contribution to sulphur dioxide production in the marine atmosphere. *Atmospheric Chemistry and Physics*, *22*(9), 6309–6325. https://doi.org/10.5194/acp-22-6309-2022

Perraud, V., Meinardi, S., Blake, D. R., & Finlayson-Pitts, B. J. (2016). Challenges associated with the sampling and analysis of organosulfur compounds in air using real-time PTR-ToF-MS and offline GC-FID. *Atmospheric Measurement Techniques*, *9*(3), 1325–1340. https://doi.org/10.5194/amt-9-1325-2016

Quinn, P. K., & Bates, T. S. (2011). The case against climate regulation via oceanic phytoplankton sulphur emissions. *Nature*, *480*, 51–56. https://doi.org/10.1038/nature10580

Rocco, M., Dunne, E., Peltola, M., Barr, N., Williams, J., Colomb, A., et al. (2021). Oceanic phytoplankton are a potentially important source of benzenoids to the remote marine atmosphere. *Communications Earth & Environment*, *2*(1), 175. https://doi.org/10.1038/s43247-021-00253-0

Saint-Macary, A. D., Marriner, A., Barthelmeß, T., Deppeler, S., Safi, K., Costa Santana, R., et al. (2023). Dimethyl sulfide cycling in the sea surface microlayer in the southwestern Pacific–Part 1: Enrichment potential determined using a novel sampler. *Ocean Science*, *19*(1), 1–15. https://doi.org/10.5194/OS-19-1-2023

Saltzman, E. S., King, D. B., Holmen, K., & Leck, C. (1993). Experimental determination of the diffusion coefficient of dimethylsulfide in water. *Journal of Geophysical Research*, *98*(C9), 16481–16486. https://doi.org/10.1029/93JC01858

Sander, R., Acree Jr, W. E., De Visscher, A., Schwartz, S. E., & Wallington, T. J. (2022). Henry's law constants (IUPAC Recommendations 2021). *Pure and Applied Chemistry*, *94*(1), 71–85. https://doi.org/10.1515/pac-2020-0302

Schneider, S. R., Lakey, P. S. J., Shiraiwa, M., & Abbatt, J. P. D. (2020). Reactive uptake of ozone to simulated seawater: Evidence for iodide depletion. *Journal of Physical Chemistry A*, *124*(47), 9844–9853. https://doi.org/10.1021/acs.jpca.0c08917

Schwinger, J., Tjiputra, J., Goris, N., Six, K. D., Kirkevåg, A., Seland, Ø., et al. (2017). Amplification of global warming through pH dependence of DMS production simulated with a fully coupled Earth system model. *Biogeosciences*, *14*(15), 3633–3648. https://doi.org/10.5194/BG-14-3633-2017

Sellegri, K., Harvey, M., Peltola, M., Saint-Macary, A., Barthelmeß, T., Rocco, M., et al. (2023). Sea2Cloud: From biogenic emission fluxes to cloud properties in the Southwest Pacific. *Bulletin of the American Meteorological Society*, *104*(5), E1017–E1043. https://doi.org/10.1175/BAMS-D-21-0063.1

Shaw, D. K., Sekar, J., & Ramalingam, P. V. (2022). Recent insights into oceanic dimethylsulfoniopropionate biosynthesis and catabolism. *Environmental Microbiology*, *24*(6), 2669–2700. https://doi.org/10.1111/1462-2920.16045

Simó, R., Grimalt, J. O., Pedros-Alio, C., & Albaiges, J. (1995). Occurrence and transformation of dissolved dimethyl sulphur species in stratified seawater (western mediterranean sea). *Marine Ecology Progress Series*, *127*(1–3), 291–299. https://doi.org/10.3354/MEPS127291

Simó, R., & Dachs, J. (2002). Global Ocean emission of dimethylsulfide predicted from biogeophysical data. *Global Biogeochemical Cycles*, *16*(4), 26–31. https://doi.org/10.1029/2001GB001829

Sinha, V., Williams, J., Meyerhöfer, M., Riebesell, U., Paulino, A. I., & Larsen, A. (2007). Air-Sea fluxes of methanol, acetone, acetaldehyde, isoprene and DMS from a Norwegian Fjord following a phytoplankton bloom in a mesocosm experiment. *Atmospheric Chemistry and Physics*, *7*(3), 739–755. https://doi.org/10.5194/ACP-7-739-2007

Stefels, J., Steinke, M., Turner, S., Malin, G., & Belviso, S. (2007). Environmental constraints on the production and removal of the climatically active gas dimethylsulphide (DMS) and implications for ecosystem modelling. *Biogeochemistry*, *83*(1–3), 245–275. https://doi.org/10.1007/S10533-007-9091-5/TABLES/6

Stefels, J., Van Leeuwe, M. A., Jones, E. M., Meredith, M. P., Venables, H. J., Webb, A. L., & Henley, S. F. (2018). Impact of sea-ice melt on dimethyl sulfide (sulfoniopropionate) inventories in surface waters of Marguerite Bay, West Antarctic Peninsula. *Philosophical Transactions of the Royal Society A: Mathematical, Physical & Engineering Sciences*, *376*(2122), 20170169. https://doi.org/10.1098/rsta.2017.0169

Steinke, M., Daniel, C., & Kirst, G. O. (1996). DMSP lyase in marine macro-and microalgae: Intraspecific differences in cleavage activity. In *Biological and environmental chemistry of DMSP and related sulfonium compounds* (pp. 317–324). https://doi.org/10.1007/978-1-4613-0377-0_27

Stramski, D., Bricaud, A., & Morel, A. (2001). Modeling the inherent optical properties of the ocean based on the detailed composition of the planktonic community. *Applied Optics*, *40*(18), 2929–2945. https://doi.org/10.1364/ao.40.002929

Taylor, B. F., & Visscher, P. T. (1996). Metabolic pathways involved in DMSP degradation. In *Biological and environmental chemistry of DMSP and related sulfonium compounds* (pp. 265–276). Springer US. https://doi.org/10.1007/978-1-4613-0377-0_23

Thornton, D. C. O. (2014). Dissolved organic matter (DOM) release by phytoplankton in the contemporary and future ocean. *European Journal of Phycology*, *49*(1), 20–46. https://doi.org/10.1080/09670262.2013.875596

Tinel, L., Adams, T. J., Hollis, L. D. J., Bridger, A. J. M., Chance, R. J., Ward, M. W., et al. (2020). Influence of the Sea surface microlayer on oceanic iodine emissions. *Environmental Science and Technology*, *54*(20), 13228–13237. https://doi.org/10.1021/acs.est.0c02736

Tinel, L. J. A., Saltzman, E., Engel, A., Fernandez, R., Li, Q., Mahajan, A. S., et al. (2023). Impacts of ocean biogeochemistry on atmospheric chemistry. *Elementa: Science of the Anthropocene*, *11*(1), 00032. https://doi.org/10.1525/elementa.2023.00032

Townsend, D. W., & Keller, M. D. (1996). Dimethylsulfide (DMS) and dimethylsulfoniopropionate (DMSP) in relation to phytoplankton in the Gulf of Maine. *Marine Ecology Progress Series*, *137*(1–3), 229–241. https://doi.org/10.3354/MEPS137229

Uitz, J., Claustre, H., Morel, A., & Hooker, S. B. (2006). Vertical distribution of phytoplankton communities in open ocean: An assessment based on surface chlorophyll. *Journal of Geophysical Research*, *111*(C8). https://doi.org/10.1029/2005JC003207

Vogt, M., Vallina, S. M., Buitenhuis, E. T., Bopp, L., & Le Quéré, C. (2010). Simulating dimethylsulphide seasonality with the dynamic green ocean model PlankTOM5. *Journal of Geophysical Research*, *115*(C6), 6021. https://doi.org/10.1029/2009JC005529

Walker, C. F., Harvey, M. J., Smith, M. J., Bell, T. G., Saltzman, E. S., Marriner, A. S., et al. (2016). Assessing the potential for dimethylsulfide enrichment at the sea surface and its influence on air–sea flux. *Ocean Science*, *12*(5), 1033–1048. https://doi.org/10.5194/os-2016-26

Wang, W. L., Song, G., Primeau, F., Saltzman, E. S., Bell, T. G., & Moore, J. K. (2020). Global ocean dimethyl sulfide climatology estimated from observations and an artificial neural network. *Biogeosciences*, *17*(21), 5335–5354. https://doi.org/10.5194/BG-17-5335-2020

Wanninkhof, R. (2014). Relationship between wind speed and gas exchange over the ocean revisited. *Limnology and Oceanography: Methods*, *12*(6), 351–362. https://doi.org/10.4319/LOM.2014.12.351

Wohl, C., Brown, I., Kitidis, V., Jones, A. E., Sturges, W. T., Nightingale, P. D., & Yang, M. (2020). Underway seawater and atmospheric measurements of volatile organic compounds in the Southern Ocean. *Biogeosciences*, *17*(9), 2593–2619. https://doi.org/10.5194/bg-17-2593-2020

Wolfe, G. V., & Steinke, M. (1996). Grazing-activated production of dimethyl sulfide (DMS) by two clones of Emiliania huxleyi. *Limnology & Oceanography*, *41*(6), 1151–1160. https://doi.org/10.4319/lo.1996.41.6.1151

Woodhouse, M. T., Mann, G. W., Carslaw, K. S., & Boucher, O. (2013). Sensitivity of cloud condensation nuclei to regional changes in dimethylsulphide emissions. *Atmospheric Chemistry and Physics*, *13*(5), 2723–2733. https://doi.org/10.5194/ACP-13-2723-2013

Yang, G. P., Levasseur, M., Michaud, S., & Scarratt, M. (2005). Biogeochemistry of dimethylsulfide (DMS) and dimethylsulfoniopropionate (DMSP) in the surface microlayer and subsurface water of the western North Atlantic during spring. *Marine Chemistry*, *96*(3–4), 315–329. https://doi.org/10.1016/j.marchem.2005.03.003

Yassaa, N., Colomb, A., Lochte, K., Peeken, I., & Williams, J. (2006). Development and application of a headspace solid-phase microextraction and gas chromatography/mass spectrometry method for the determination of dimethylsulfide emitted by eight marine phytoplankton species. *Limnology and Oceanography: Methods*, *4*(10), 374–381. https://doi.org/10.4319/LOM.2006.4.374

Yoch, D. C. (2002). Dimethylsulfoniopropionate: Its sources, role in the marine Food Web, and biological degradation to dimethylsulfide. *Applied and Environmental Microbiology*, *68*(12), 5804–5815. https://doi.org/10.1128/AEM.68.12.5804-5815.2002/ASSET/25DF11FF-AA0B-4EC6-8354-644C1B28F32C/ASSETS/GRAPHIC/AM1220922002.JPEG

Zhang, M., Marandino, C. A., Yan, J., Lin, Q., Park, K., & Xu, G. (2021). DMS sea-to-air fluxes and their influence on sulfate aerosols over the Southern Ocean, south-east Indian Ocean and north-west Pacific Ocean. *Environmental Chemistry*, *18*(6), 193–201. https://doi.org/10.1071/EN21003